Surface Nucleation Theory for Chain-Folded Systems with Lattice Strain: Curved Edges

John D. Hoffman* and Robert L. Miller*

Michigan Molecular Institute, 1910 W St. Andrews Road, Midland, Michigan 48640.
Received May 24, 1988; Revised Manuscript Received October 25, 1988

ABSTRACT: To provide a foundation for understanding the origin of chain-folded crystals with curved edges, nucleation theory has been generalized to include (1) the effect of lattice strain and the concomitant nonideal surface or niche and (2) the nucleation and growth properties associated with a growth face that is serrated on a *molecular* level, rather than flat as in prior treatments. Expressions for the substrate completion rate, the growth rates in regimes I, II, and III, and the initial lamellar thickness are given for each type of surface (i.e., flat or serrated) for the important variants of items 1 and 2. (Each model is treated assuming both steady-state and non-steady-state nucleation; the results for a specified type of surface are very similar.) Emphasis is given to situations that lead to a reduced substrate completion rate, since it has been shown that a sector with a curved edge (section of an ellipse) will arise when the substrate completion rate of that sector is only slightly larger than the rate of advance of the adjoining sector. It is found that the presence of lattice strain (arising from a bulkiness of the chain folds) provides the required mechanism. The model with a serrated growth face, and with a nonideal surface resulting from lattice strain, leads to an explanation of the curved edges exhibited by the 200 sector in certain polyethylene single crystals that have both 110- and 200-type sectors. (The theory also explains the "double" melting points exhibited by such crystals.) The ability to accommodate curved edges removes an objection that has been raised concerning the validity of nucleation theory as applied to crystallization with chain folding. A discussion is given concerning the physical significance of the apportionment parameter Ψ.

I. Introduction

Our overall objective is to modify and extend nucleation theory so that it is applicable to a wider variety of polymer crystallization phenomena than was heretofore possible. In particular, we outline a theoretical basis for understanding the origin of chain-folded crystals with curved edges. To do this we introduce lattice strain effects through an interfacial surface free energy σ_s, which in general reduces the melting point of the sector involved and also lowers the substrate completion rate. We also treat a "serrated" substrate in addition to the customary "flat surface" substrate. The "serrated surface" model with lattice strain is successful in explaining the curved edges exhibited by the 200-type sectors of certain polyethylene single crystals.

The importance of dealing with the problem of polymer single crystals with curved edges (specifically polyethylene in our case) arises from the fact that nucleation theory has heretofore been unable to explain the origin of such edges. This led some investigators to have doubts about the nucleation-based kinetic theory of polymer crystal growth with chain folding. Thus, though nucleation theory even in its simplest form was able to explain such centrally important phenomena as the growth rates in the various regimes of crystallization and the initial lamellar thickness (fold period) in terms of a unified flux equation approach (see, e.g., ref 1), a concern was growing that this approach might harbor some serious inner flaw.

It is well here to review the background briefly. The lateral growth habits of lamellar crystals of polyethylene grown from solution have long been known to vary depending on growth temperature and/or undercooling, concentration, and molecular weight, as well as the nature of the solvent (see, e.g., ref 2 for an extensive bibliography). Those habits that reflect changes in the ratio of the growth rates of the 110 and 200 faces have generally been characterized in terms of the axial ratio of the single crystals. Passaglia and Khoury[2] applied the kinetic theory of polymer crystal growth in an analysis of the variations of the lateral growth habits exhibited by polyethylene single crystals formed in xylene at specified isothermal growth temperatures; in this work the aspect ratios treated ranged from 0.66 (lamellae bounded only by four 110 faces) to 1.09 (six-sided lamellae bounded by four 110 faces and two 200 faces). These authors specifically pointed out that their analysis did not extend to crystals grown in poor solvents at higher temperatures, which exhibited high aspect ratios (e.g., greater than 2) and in which the 200 faces exhibit distinctly curved profiles. The origin of the "curved edge" feature and the corresponding large aspect ratio of such crystals thus remain to be accounted for. The concern about the apparent inability of nucleation theory to accommodate the existence of curved edges is reflected, for example, in the work of Sadler (see ref 3 and references therein).

In view of the above we present here an expanded version of nucleation theory designed to deal with the question of curved edges. This approach features a consideration of lattice strain effects arising from chain-fold repulsions, which strain lowers the melting point and reduces the substrate completion rate of the affected sector. The lattice strain effect is introduced through an interfacial surface free energy σ_s. The paper also includes a treatment of a crystal that has a "serrated" face (serrated *on a molecular level*), as appears to be appropriate to the 200 sectors of polyethylene, rather than the customary "flat surface" growth front. The need to identify and treat nucleation models that predict a considerably reduced substrate completion rate is based on the phenomenological crystal growth treatment of Mansfield,[4] who showed that a sector with a markedly curved edge (section of an ellipse) will appear when the substrate completion rate of that sector is only slightly larger than the rate of advance of the adjoining sector. We shall show that the serrated surface model with lattice strain has precisely this property as well as other features that are essential to the treatment of the curved edges in polyethylene single crystals. This model will be employed in an analysis of the data of Organ and Keller,[5] who have provided explicit values of the aspect ratio, curvature, and growth rate of polyethylene single crystals as a function of crystallization temperature in *n*-hexadecane; the crystals studied were formed at relatively high growth temperatures and exhibited large aspect ratios and distinct curvature on the 200 faces. A more

0024-9297/89/2222-3038$01.50/0

detailed analysis of the results of Organ and Keller for crystals formed in both *n*-hexadecane and *n*-tetradecanol will be published elsewhere.[6] Given the extensive data provided by Organ and Keller, the treatment goes well beyond predicting the shape of the curved edge and the axial ratio of the crystals as a function of undercooling; for example, it yields precise values of the interfacial surface free energy σ_s and the fold surface free energy $\sigma_{e(200)}$ of the 200 sector and correctly predicts that the 200 sector will melt prior to the 110 on warming.

Nucleation theory is customarily applied to chain-folded crystallization by assuming full activity of both the forward (stem addition) and backward (stem removal) reactions.[1,7,8] This approach assumes detailed balance and treats surface nucleation as a steady-state process. Detailed balance must certainly hold for extended-chain crystallization at or very near the melting point but is not necessarily required at the relatively large undercoolings typical of polymer crystallization with chain folding. At such undercoolings the backward reaction may be strongly subdued, in which case surface nucleation is to be viewed as a non-steady-state process. In a previous paper, we mentioned physical reasons based on the analogy with the slow rates of polymer desorption from surfaces why the backward reaction may be sluggish.[9] In the present work we give expressions for the essential results for the models with lattice strain included for the case where the backward reaction is subdued. (One reason for considering the case with a subdued backward reaction is that Guttman and DiMarzio were able to predict the existence of regimes I, II, and III for the "bricklayer" surface model using only forward reactions.[10] Another is that from personal communications we are aware that certain investigators are curious to know if the non-steady-state case differs in any significant manner from that where steady-state nucleation obtains.) It is important early on in the present paper to emphasize that there is little difference in the results for a given surface model if the backward reaction is included in full on the one hand or omitted on the other. We have previously shown such a result for the "flat surface" model in the absence of lattice strain.[9] The somewhat simpler derivations involving only forward reactions for the flat surface and serrated surface models with lattice strain are employed in the body of the text. The corresponding treatment where the backward reactions are fully active is outlined in Appendix A. In general, the non-steady-state calculations with a subdued backward reactions are denoted $\epsilon = 0$, and the steady-state cases featuring a fully active backward reaction are denoted $\epsilon = 1$.

In the course of the treatment of the flat surface and the serrated surface models, we shall mention the so-called "apportionment factor" Ψ. Here we propose to elucidate the physical origin of this factor; we deem this important because Ψ has sometimes been thought to represent an arbitrary feature of nucleation theory. It is this factor that decides what fraction of the free energy of fusion is given up at the instant in time that the activated state is reached as a stem (or parts of it) are put down on the substrate. Actual values of Ψ are evidently in the vicinity of $^1/_3$ or less. Most of our calculations will be made on the basis $\Psi = 0$, since this avoids unnecessary complication and gives results in the moderate undercooling range of interest here that are numerically virtually identical with those found with the more complicated expressions with, say, $\Psi = {}^1/_3$. Values of $\Psi = 0$ to $\Psi = {}^1/_3$ in general avoid the prediction of the so-called "δ catastrophe", where at a large undercooling the flux and the initial lamellar thickness rather abruptly depart from normal behavior and approach infinity.[1] The "δ catastrophe" effect has not been observed experimentally, but we deliberately retain the factor Ψ in the theory in its most general form to accommodate such an effect should it be found and for the compelling reason that a Ψ value near 0.38 is definitely required to deal with the lamellar thickness data for *it*-polystyrene crystals at very large undercoolings (see later). In particular, we show that a value of Ψ below unity has the general meaning that at the instant in time that the activated state is achieved in the forward reaction involving stem addition, only part of the stem is crystallographically attached to the substrate. This "partial stem" feature has not been fully emphasized hitherto.

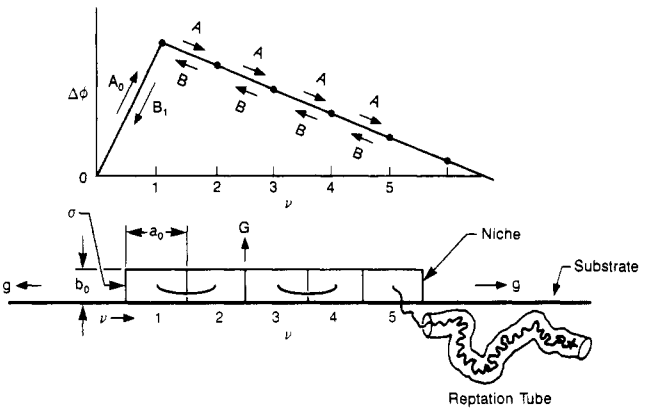

Figure 1. Model for nucleation and substrate completion on a flat surface. The forward reaction for the first ($\nu = 1$) stem is opposed by a free energy barrier $2b_0[\sigma + (a_0/2b_0)\sigma_s]l$, or $\sim 2b_0[\sigma + \sigma_s/2]l$ for the case $a_0 \approx b_0$. Each stem added to the substrate involves the free energy $q_{fold} + (a_0 + b_0)\sigma_s l$, where σ_s represents the nonideal character of the "niche". The strain-free case corresponds to $\sigma_s = 0$.

The treatment in the body of the paper deals with crystallization from the melt. The changes required to adapt the results to crystallization in dilute solution are noted. Though detailed experimental studies yielding curvature, aspect ratio, and growth rate data sufficient for an analysis have to date been confined to dilute solution (e.g., the studies of Organ and Keller[5]), we judge that the basic theory may well apply to certain melt-crystallized systems as well. We note that "elliptical" lamellae, which may be analogous to those obtained from dilute solution, have recently been found in melt-crystallized polyethylene.[11]

The overall plan of the paper is as follows. The customary "flat surface" model is treated first (section II). This allows the apportionment factor Ψ, the curtailment of the backward reaction, and lattice strain effects to be discussed in a familiar framework. Next, the "serrated surface" model is introduced and treated in a parallel manner (section III). The serrated model with lattice strain is then employed in section IV to explain the curved edges in certain polyethylene crystals. The discussion in section V summarizes the results and places the work in a more general perspective.

II. Nucleation on a Nonideal (Strained) Flat Surface

(A) Model: Bulk and Surface Thermodynamics. The model employed for the calculations for the "flat surface" model with lattice strain is shown in Figure 1. The chain folds in the substrate and in the bulk of the crystal below it are assumed to repel each other in such a manner that the lattice undergoes a general expansion. (We shall justify this approach in some detail subsequently.) This renders both the substrate and the interior

lattice nonideal with respect to the situation where there is no repulsion of the chain folds. From an energetic standpoint, we characterize this effect by an interfacial surface free energy σ_s, which is in erg cm^{-2}. The counting method employed here is that each stem shares the interfacial energy with its neighbors, which is equivalent to each stem contributing $(a_0 + b_0)\sigma_s l$. The free energy increase per unit volume ("lattice strain energy") in the crystal proper resulting from the lattice expansion is (on a per stem basis) given by $(a_0 + b_0)\sigma_s l$ divided by the volume of a stem $a_0 b_0 l$; this comes to $(a_0 + b_0)\sigma_s/a_0 b_0$, which is in erg cm^{-3}. (This counting method will prove to be consistent with the surface energetics associated with the attachment of stems in the primary nucleation and substrate completion acts that comprise the surface nucleation process to be discussed shortly.) The quantities a_0 and b_0, which are in centimeters, are defined in Figure 1: the quantity $a_0 b_0$ is the cross-sectional area of the chain. The quantity l is taken as a variable and represents the lamellar thickness or, more precisely, the stem length between the two fold surfaces if tilt is present. The free energy of fusion, i.e., the free energy difference between the subcooled liquid and the crystal with lattice strain energy included is given by

$$\Delta G_s = \Delta G - (a_0 + b_0)\sigma_s/a_0 b_0 = (\Delta h_f)(\Delta T_s)/T_m \quad (1a)$$

where

$$\Delta G = (\Delta h_f)(\Delta T)/T_m \quad (1b)$$

and Δh_f is the heat of fusion. Here ΔG is the normal free energy of fusion in erg cm^{-3} in the absence of lattice strain, ΔG_s the free energy of fusion in the same units in the presence of lattice strain, T_m the melting point of a large, strain-free, extended-chain crystal of the molecular weight under consideration, $\Delta T = T_m - T_x$ the undercooling relative to that strain-free crystal, and $\Delta T_s = T_s - T_x$ the undercooling relative to a crystal with lattice strain. We shall shortly give an expression for T_s, which is lower than T_m when $\sigma_s > 0$.

The interfacial surface free energy σ_s, which is so to speak "buried" in the lattice proper, has a definite effect on the melting point of a thin lamellar crystal. By considering an isolated chain-folded crystal of thickness l that is very large in the other two dimensions, one can readily derive from eq 1 under the condition $\Delta G_s = 0$ that the melting point is

$$T_m' = T_m\left\{1 - \frac{2\sigma_e}{(\Delta h_f)l} - \frac{(a_0 + b_0)\sigma_s}{(\Delta h_f)a_0 b_0}\right\} \quad (2a)$$

where σ_e is the *mean* fold surface free energy in erg cm^{-2}. This reduces to the formula usually employed when one sets $\sigma_s = 0$. The expression $T_m[1 - (a_0 + b_0)\sigma_s/(\Delta h_f)a_0 b_0]$ represents the melting point T_s of an extended-chain crystal containing the lattice strain energy $(a_0 + b_0)\sigma_s/a_0 b_0$. The effective undercooling ΔT_s that holds for the sector of a crystal that exhibits lattice strain is then

$$\Delta T_s = T_s - T_x = T_m[1 - (a_0 + b_0)\sigma_s/(\Delta h_f)a_0 b_0] - T_x \quad (2b)$$

In the above, $T_x = T$ is the isothermal crystallization temperature.

As a useful orientation we give estimates of the quantities of interest to show the effect of σ_s on the bulk properties of a system with lattice strain. We would suppose that σ_s (if it is present at all) would be considerably less than σ. For illustrative purposes we assume $\sigma_s = 1.5$ erg cm^{-2}, which with[1] $\sigma = 12$ erg cm^{-2} gives $\sigma_s/\sigma = 0.125$. With the nominal values $a_0 = 5 \times 10^{-8}$ cm and $b_0 = 4 \times 10^{-8}$ cm, the lattice strain energy comes to 6.75×10^7 erg cm^{-3}. This is only 2.7% of the heat of fusion if the latter is taken to have the typical value 2.5×10^9 erg cm^{-3}. The effect of σ_s on the melting point T_m' in eq 2a is significant. If one takes $T_m = 420$ K, the additional reduction in T_m' caused by σ_s is $\sim$11.34 °C for the numerical values cited above. Though no such large depression is known for any case where the flat surface model is applicable, an example involving the serrated model where such does occur will be given in section IV.

It is pertinent to mention certain facts that support the thermodynamic aspects of the model with lattice strain. In writing eq 1a we have in effect asserted that chain-fold repulsions can cause a general expansion of the lattice. There exists direct confirmation that this is true in the key work of Davis and co-workers.[12] These investigators demonstrated by careful X-ray studies that a general expansion of the lattice occurred in both solution- and melt-crystallized polyethylene that was largely attributable to repulsion effects on the lamellar surface. The expansion effect, though small, was greater the smaller the fold period. (A similar but considerably smaller general lattice expansion was found in the *n*-paraffins[12] owing to the repulsion of the $-CH_3$ end groups, the effect being most noticeable for short chains.) We conclude that a surface effect (repulsion of chain folds) leads to a resultant effect in the lattice proper in chain-folded polymers that must certainly increase the bulk free energy of the crystal interior. Accordingly we feel justified in writing that part of the total bulk free energy due to the "buried" interfacial free energy per stem as a function of l, i.e., as $(a_0 + b_0)\sigma_s l$; this expression was employed earlier in $(a_0 + b_0)\sigma_s l$ divided by $a_0 b_0 l$ to obtain the lattice strain energy, i.e., the stored strain-induced free energy per unit volume, in ΔG_s. It is to be noted that σ_s might depend to some extent on the lamellar thickness l_g^*, the value of σ_s probably being somewhat smaller for larger l_g^*. We therefore stipulate in what follows that σ_s is to be regarded as an average value for the l_g^* range under consideration.

A further justification for the model is to be found in molecular energy calculations. With the help of the lattice expansion data of Davis and co-workers[12] on melt-crystallized polyethylene (which contains a significant fraction of 200-type folds) and appropriate potential energy functions, Marand[13] has estimated values of σ_s in the range of 1.0 erg cm^{-2}. This shows that σ_s is not an ad hoc fitting parameter, but rather a quantity that has a direct physical interpretation.

From the above, we deem the thermodynamic aspects of the lattice strain model to be on a sound basis. To this we may add, in anticipation of the proof, that the above estimate of σ_s from molecular energy calculations is well within a factor of 2 of the σ_s value that explains the curvature and aspect ratio data of Organ and Keller for polyethylene single crystals formed in dilute solution.

Before setting down the thermodynamics of the formation of a surface nucleus that will feature the fold surface free energy σ_e, it is well to comment on this quantity. One purpose is to point out that we do not intend to imply "perfect" chain folding with totally adjacent reentry in our models. Another is to note that there is a definite lower bound of topological origin on the amount of "tight" folding that justifies the use of a model that is basically of the chain-folded type. Note that σ_e (sometimes denoted elsewhere[14] as $\bar{\sigma}_e$) has been defined above as the *mean* surface free energy associated with the fold surface. In this context, σ_e includes a major contribution from "tight" folds and lesser contributions from

such imperfections as nonadjacent reentrant folds, short cilia, chain ends, and the few interlamellar tie molecules. For the case of vertical stems, the "gambler's ruin" calculation shows that for topological reasons close to two-thirds of the surface must consist of "tight" folds, i.e., folds that connect adjacent or very near adjacent stems with no amorphous character in the traverse between them.[15-17] For normal fold energies, about half of the tight folds are predicted to be strictly adjacent,[18] and this is confirmed for quench-crystallized polyethylene by neutron-scattering studies.[19] The "gambler's ruin" lower bound of about two-thirds tight folds is exceeded for crystals formed from dilute solution but appears to be approached in specimens quench-crystallized from the melt.[17,19] The energetically favorable "niche" exhibited by the flat surface model (Figure 1) together with the paucity of competing molecules is one major reason for the relatively high degree of strict adjacency in single crystals formed from dilute solution. In any event, the σ_e used in the expressions to follow is a mean value that includes the effect of imperfections, and its value may tend to fall noticeably below that attributable to the hypothetical perfect or nearly perfect chain-folded surface.

Consider now the energetics of the formation of a surface nucleus on a flat surface substrate that itself exhibits lattice strain resulting from the repulsion of chain folds. By reference to Figure 1, one can write the free energy of formation as follows:

$$\Delta\phi_\nu = 2b_0\sigma l + \nu a_0\sigma_s l + (\nu - 1)b_0\sigma_s l + 2(\nu - 1)a_0b_0\sigma_e - \nu a_0b_0 l(\Delta G) \quad (3a)$$

In this expression σ is the lateral surface free energy in erg cm^{-2}, $2a_0b_0\sigma_e$ the effective work of chain folding q, ΔG the free energy of fusion as given by eq 1b, and ν the number of stems added to the substrate. Notice from the appearance of ΔG that we employ the unstrained crystal in defining the reference state. The term $2b_0\sigma l$ is the total work in forming the two exposed sides of the first ($\nu = 1$) stem. The term $\nu a_0\sigma_s l$ gives the extra work done in putting each stem down, including the first one, because of the interfacial free energy resulting from lattice strain in the substrate. The quantity $(\nu - 1)b_0\sigma_s l$ represents the interfacial effect on the lateral surface as each stem (other than the first) is added during the substrate completion process. The term $2(\nu - 1)a_0b_0\sigma_e$ gives the work of chain folding for the stems added after the first. Finally the term $-\nu a_0b_0 l(\Delta G)$ represents the total decrease in free energy, after the system settles down, upon the addition of ν stems.

To obtain a convenient working equation, we rewrite eq 3a as

$$\Delta\phi_\nu = 2b_0\sigma l + a_0\sigma_s l - a_0b_0 l(\Delta G) - (\nu - 1)a_0b_0\left\{l\left[(\Delta G) - \frac{(a_0 + b_0)\sigma_s}{a_0b_0}\right] - 2\sigma_e\right\} \quad (3b)$$

This expression reduces to that commonly employed to treat the flat surface model when σ_s is set equal to zero. Note that the two terms in the brackets in eq 3b restate the definition of ΔG_s of eq 1a.

We have intentionally omitted a term $\lambda kT \ln (l_0/x_0)$, which describes the free energy change accompanying the attachment of the first stem. This term is mainly important in predicting details of the molecular weight dependence of the crystallization rate,[9] but its omission has no important effect in what follows.

(B) Rate Constants, Flux Equations, Nucleation Rate, Initial Lamellar Thickness, and Substrate Completion Rate. General Rate Constants. We now construct the expressions that control the rates of stem addition and stem removal (if such occurs) on a general basis. We initially assume detailed balance, so the rate constants must be consistent with eq 3b. We write the rate constants A_0, B_1, A, and B shown in Figure 1 in such a manner as to expose ΔG_s directly, since in calculating the total flux S_T we shall perform an integration that involves ΔG_s. The introduction of an apportionment factor Ψ below is patterned after its original application.[20] Subsequently, we shall introduce certain simplifications and proceed to calculate the desired quantities.

The rate expression for the forward reaction that puts down the first ($\nu = 1$) stem is

$$A_0 = \beta e^{-[2b_0\sigma + a_0\sigma_s]l/kT} e^{\Psi[a_0b_0(\Delta G_s) + (a_0 + b_0)\sigma_s]l/kT} \quad (4a)$$

The factor $\exp[-2b_0\sigma + a_0\sigma_s]l/kT$ is by far the most important factor in determining the nucleation rate i. The backward reaction corresponding to removal of the first stem is

$$B_1 = \beta e^{-(1-\Psi)[a_0b_0(\Delta G_s) + (a_0 + b_0)\sigma_s]l/kT} \quad (4b)$$

The ratio A_0/B_1 recovers the equilibrium distribution for $\nu = 1$ in eq 3b, so that detailed balance is preserved. The factor β, which is in events per second, represents the retardation resulting from the transport of a polymer chain through the liquid to the growth front. For crystallization from the melt at moderate undercoolings, β varies approximately as $(1/n)\exp(-Q_D^*/RT)$, where n is the number of chain units and Q_D^* is the activation energy of reptation in the melt.[9,21] Modifications in the form just given for β are required at low temperatures or if crystallization from solution is considered (see later). The numerical factor Ψ multiplying what is in effect $a_0b_0l(\Delta G)$ in eq 4a is a measure of that fraction of the free energy of fusion that is given up at the instant in time the activation barrier $[2b_0\sigma + a_0\sigma_s]l$ is incurred. Values of Ψ are formally restricted to be between zero and unity and are expected to be $\sim 1/3$ (see later).

The forward reaction in the substrate completion process ($\nu \geq 2$) is given by

$$A = \beta e^{-q/kT} e^{-(a_0 + b_0)\sigma_s l/kT} e^{\Psi[a_0b_0(\Delta G_s) + (a_0 + b_0)\sigma_s]l/kT} \quad (4c)$$

where $q = 2a_0b_0\sigma_e$ is the mean work of chain folding. The substrate completion process is thus opposed by the necessity of forming the chain folds and, for the current model, the requirement that the interfaces involving σ_s be formed. (It is also opposed by the liquid-state retardations represented by β.) The process is promoted by the free energy of fusion to the extent permitted by the value of Ψ. The backward reaction for the removal of the terminal stem is given by

$$B = B_1 = \beta e^{-(1-\Psi)[a_0b_0(\Delta G_s) + (a_0 + b_0)\sigma_s]l/kT} \quad (4d)$$

Here β has the same meaning as given above, and the Ψ in eq 4d is a measure of the fraction of the free energy of fusion that is given up at the instant in time that the chain fold is formed. It is easy to see that if the fold forms rather early in the overall process before much of the stem is crystallographically attached, then low values of Ψ will result. This leads to a molecular interpretation of Ψ. The ratio A/B is seen to preserve detailed balance when compared with eq 3b for $\nu \geq 2$.

Equations 4 provide a general basis for developing expressions for the initial lamellar thickness l_g^*, the nucleation rate i, and the substrate completion rate g. From the latter two quantities one can readily develop formulas for G_I, G_{II}, and G_{III}, the growth rates in regimes I, II, and III, respectively. These calculations are most readily carried out with an accuracy sufficient for applications with

the help of certain approximations whose physical significance can be stated and for which the quantitative effect can be assessed. The first of these approximations is that which takes Ψ to be small or zero; this will be discussed shortly. The second is that which subdues the backward reaction, i.e., sets $B = B_1 \simeq 0$. At normal undercoolings, the essential results for experimentally determinable variables such as G_I, G_{II}, G_{III}, g, or l_g^* obtained with the approximations are numerically very similar to those obtained without them.

Physical Origin and Value of Ψ. To simplify the discussion below, we deal with the case $\sigma_s \rightarrow 0$. At the outset we can say that physically realistic values of Ψ originate from the fact that an entire stem is *not* put down instantaneously either as a rigid unit or in a simple "stitching down" process that begins at one side of the substrate and proceeds in consecutive monomer-by-monomer fashion to the other.

Consider first the case of the substrate completion process ($\nu \geq 2$). Here, to put the chain fold and the entire stem down at the same instant would require the work of chain folding q and the full free energy of fusion $a_0b_0l(\Delta G)$ to be incurred simultaneously. This unrealistic "rigid stem" picture leads to $\Psi = 1$ as inspection of eq 4c shows. It also leads, when detailed balance prevails, to the odd situation in eq 4d where no free energy of fusion opposes the removal of a stem. The regular "stitching down" concept has the fold forming first, giving $\Psi = 0$; this too is clearly oversimplified. It is more likely during the substrate completion process that the fold forms fairly early in the process, say when a third of the stem has been put down in the niche. This physical situation is represented in eq 4c as $\Psi = {}^1/_3$. *One recognizes here that a Ψ value below unity implies a "partial stem" character in the activated state involved in substrate completion.* After the activated state is reached, the other two-thirds of the stem attaches in a short time and forms a new and complete niche. To remove this now fully attached stem, the amount $(1 - \Psi)a_0b_0l(\Delta G)$, or two-thirds of the free energy of fusion, must be supplied as seen from eq 4d. The foregoing gives a physical picture of the origin of Ψ in the substrate completion process. It renders plausible the concept that Ψ for the substrate completion process will be quite small. It also highlights the fact that the activated state controlling the rate of the forward reaction involves the crystallographic attachment of only *part* of a full stem; the rest of the stem goes down, forming a complete niche, in a rapid subsequent process. The resultant completed niche is again a relatively inviting site for the pendant molecule to execute an adjacent reentry. While some nonadjacent events will certainly occur—more so in crystallization from the melt than in dilute solution—it should be recalled that there exist irreducible topological restrictions that place a definite lower bound on the degree of tight folding.[17]

Consider now the case of the Ψ involved in the eq 4a and 4b, which expressions refer respectively to the addition and removal of the first ($\nu = 1$) stem. Again it is sufficient to deal with the case $\sigma_s \rightarrow 0$, since this illustrates the essential points. Here, as before, the physical picture of why Ψ is expected to be small is related to the fact that the main activation barrier—in this case $2b_0\sigma l$ in eq 4a—is incurred *before* the stem is everywhere crystallographically attached, i.e., well before the full free energy of fusion $a_0b_0l(\Delta G)$ is attained. While the details are different, this parallels the general situation described above for the substrate completion process $\nu \geq 2$. Both the highly simplistic "rigid rod" and regular "stitching down" picture of the deposition of the first stem give the dubious result $\Psi = 1$. What we conceive to actually happen is that perhaps one-third of the first stem becomes crystallographically attached at various points on the substrate, corresponding to $\Psi = {}^1/_3$ in eq 4a. Simultaneously, these attachments pin much of the rest of the molecule on the surface (in a state resembling physical adsorption), thus incurring the bulk of the lateral surface free energy activation barrier $2b_0\sigma l$. (This general argument for a low-Ψ value for the first stem has been discussed previously; see pp 561–564 of ref 1.) At the instant in time that the activation barrier for the forward reaction for the first stem is attained, only a portion $\Psi = {}^1/_3$ of free energy of fusion $a_0b_0l(\Delta G)$ has been released. Hence, a Ψ below unity for the first stem bears the implication that the nature of the activated state is such that it involves a "partial stem" character just as in the case of substrate completion. After a brief interval, the first stem aligns crystallographically. This prepares it either to initiate the substrate completion process as described above or to be detached (if detailed balance holds and the backward reaction is active) according to a rate described by eq 4b with $(1 - \Psi)[a_0b_0l(\Delta G)] = {}^2/_3[a_0b_0l(\Delta G)]$. Experiments noted below support Ψ values well below unity, implying the validity of the "partial stem" character of the activated state.

In the most general case, the Ψ for the first stem may differ from that for the substrate completion process. Following earlier practice,[1,20] it is convenient to let these Ψ's have the same numerical value. This leads to useful mathematical simplification and preserves the concept that only part of a full stem is crystallographically attached when the activated state is attained, irrespective of whether the first or any subsequent stem is being considered. Consequently, B_1 in eq 4b is equal to B in eq 4d, which means that the probability in unit time of the first stem departing the surface is the same as that for a terminal stem on the substrate. This may be accepted, especially in view of the fact that the presence or absence of the backward reactions will prove to have little effect on the essential results.

Several points concerning Ψ are of importance in dealing with applications. The first is that the undercooling ΔT_c at which the so-called "δ catastrophe" is predicted to occur depends on the Ψ associated with the first stem and is found from eq 4a for the case $\sigma_s \rightarrow 0$ by setting $2b_0\sigma l$ equal to $\Psi a_0b_0l(\Delta G)$. The result is[1,20]

$$\Delta T_c = 2\sigma T_m/a_0(\Delta h_f)\Psi \qquad (5)$$

For the parameters cited earlier ($\sigma = 12$ erg cm^{-2}, $T_m = 420$ K, $a_0 = 5 \times 10^{-8}$ cm, $\Delta h_f = 2.5 \times 10^9$ erg cm^{-3}) for a polyethylene-like molecule, one gets $\Delta T_c = 80.6/\Psi$. For any reasonable value of Ψ, which we do not expect to exceed about ${}^1/_3$ for such molecules, the undercooling ΔT_c where l_g^* and the nucleation rate seriously depart from their normal behavior and approach infinity is so large ($\Delta T_c \sim 242$ °C for $\Psi = {}^1/_3$) that one hardly expects to see the "δ catastrophe" effect experimentally in such a system. This accords with the fact that this effect has never been observed, which implies that low-Ψ values are realistic.

More detailed information is available on the actual value of Ψ in two cases. Because Ψ affects the shape of the l_g^* vs ΔT curves at very large undercoolings, it is possible to obtain an estimate (or at least an upper bound) for Ψ. (The detailed theoretical expression for l_g^* vs ΔT involving Ψ is given in ref 1, pp 548 and 579.) In the case of solution-crystallized *it*-polystyrene it was found that $\Psi = 0.38$—here the undercoolings were all large and ranged up to the extraordinary value of ~190 °C (see ref 20 and ref 1, p 582). Any Ψ even slightly larger than 0.38 was

inadmissible, but a somewhat smaller one could have been employed. The data were those of Jones et al.[22] In the case of l_g^* vs ΔT data for polyethylene single crystals with predominantly 110 folds formed in xylene on the basis of data compiled by Miller,[23] it was found that $\Psi = 1$ was completely unacceptable at the larger undercoolings (see ref 20 and ref 1, p 580). Any value of Ψ from 0.7 to 0.2 fit the data very well, and $\Psi = 0$ yielded a fully acceptable fit with only slight adjustments in the behavior of σ_e. The undercooling range involved was from $\Delta T \cong 25$ °C to $\Delta T \cong 85$ °C. The ΔT_c value from eq 5 for this system is $83.3/\Psi$ in degrees centigrade and refers to the 110 face. The true value of Ψ in this instance is probably about $^1/_3$, but l_g^* data at considerably larger undercoolings would be required to determine it accurately. It is also clear that calculations based on $\Psi = 0$ give excellent results in the range of moderate undercoolings ($\Delta T \cong 25$ °C to $\Delta T = 70$ °C) in this system; there is no significant difference in the results calculated on the basis $\Psi = 0$ and $\Psi = {}^1/_3$ in this range. It is on this basis that we employ below the approximation $\Psi = 0$ for the polyethylene system. The use of the assumption $\Psi = 0$ is to be viewed as a convenient mathematical approximation that gives accurate results at the moderate undercoolings of interest and is not to be construed as meaning that none of the free energy of fusion is given up on stem attachment.

To summarize, the quantity Ψ is a parameter with a definite physical significance and is not merely an artifice that permits the δ catastrophe to be avoided. This quantity is retained in the theory in its most general form, since, as the above discussion concerning *it*-polystyrene shows, lamellar thickness data at very large undercoolings can be interpreted only with its help. The mathematical approximation $\Psi = 0$ is useful in calculating properties at normal undercoolings.

Practical Rate Constants with and without Active Backward Reaction. Using the approximation $\Psi = 0$ noted above, one gets from eq 4 the working relations for the flat surface model with lattice strain (taking into account deviation from detailed balance by introducing the factor ϵ in B and B_1):

$$A_0 = \beta e^{-[2b_0\sigma + a_0\sigma_s]l/kT} \tag{6a}$$

$$B_1 = \epsilon\beta e^{-[a_0b_0(\Delta G_s) + (a_0+b_0)\sigma_s]l/kT} \tag{6b}$$

for the first stem ($\nu = 1$) stem and

$$A = \beta e^{-q/kT} e^{-(a_0+b_0)\sigma_s l/kT} \tag{6c}$$

$$B = B_1 = \epsilon\beta e^{-[a_0b_0(\Delta G_s) + (a_0+b_0)]l/kT} \tag{6d}$$

for the substrate completion process $\nu \geq 2$. The parameter ϵ, which controls the activity of the backward reaction, is restricted to $0 \geq \epsilon \geq 1$ (see below).

The case $\epsilon = 1$ refers to the conventional situation where the backward reaction is taken to be fully active and corresponds to steady-state nucleation. Detailed balance is preserved for this case. The method of calculating l_g^*, g, i, G_I, G_{II}, and G_{III} on this basis is given in Appendix A.

In earlier work it was suggested that the backward reaction might be strongly muted.[9] This corresponds to $\epsilon \to 0$ in eq 6b and 6d, giving $B = B_1 = 0$. The assumption $\epsilon = 0$ in effect gives a stem a sticking coefficient of unity, corresponds to non-steady-state nucleation, and deals only with the forward reactions A_0 and A above. This somewhat simpler case will be worked out in the body of the text. The results for l_g^*, i, g, G_I, G_{II}, and G_{III} for $\epsilon = 0$ will prove to be very similar in all important respects to those obtained for the case of steady-state nucleation, i.e., $\epsilon = 1$, where detailed balance holds. This will become clearly apparent in a comprehensive table to be presented shortly where the results for the steady-state ($\epsilon = 1$) and non-steady-state ($\epsilon = 0$) cases for the flat surface model are compared directly. Data generally can be analyzed successfully by using either limit.

Before proceeding, it is useful to remark further on one aspect of why we have elected to exhibit the non-steady-state $\epsilon = 0$ case, where the backward reaction is assumed to be inactive in the case of chain-folded crystallization at the undercoolings typical of this phenomenon. This was in part prompted[9] by the fact that polymer molecules are exceedingly slow to desorb from surfaces even when only occasional van der Waals attachments are involved. The half-times for desorption are sometimes days or even weeks (see, e.g., ref 24). It could be argued for the $\epsilon = 1$ case of eq 4b and 4d, or alternatively eq 6b and 6d, that supplying the required fraction $1 - \Psi$ of the free energy of fusion takes care of the matter of releasing the stem from the substrate. That is to say, "supply the free energy and the terminal stem departs at that instant". However, by analogy with the case of slow desorption, we suspect that for stem removal a time factor may be involved as well. The reason that polymer desorption is so slow is not necessarily for lack of the requisite energy but may be related to the requirement that to desorb a molecule *all* the attached segments must *simultaneously* find themselves off the surface, which is statistically improbable.[25] A similar process may occur for a crystallographically attached terminal stem, which would strongly truncate the backward reaction. The lifetime of a terminal stem, i.e., the time it exists as a full stem at a "niche" before that niche is filled by a new stem, is quite short even at normal undercoolings. For example, in the case of polyethylene at the regime I → II transition at $\Delta T \cong 16.5$ °C, the substrate completion rate on the 110 face, which is not affected by any noticeable strain effects, is[9]

$$g_{110}\ (\text{cm s}^{-1}) = 8.77 \times 10^{-2}/n \tag{7}$$

where n is the number of $-CH_2-$ units in the chain. For $n = 3000$ ($M \cong 42\,000$) this gives 2.92×10^{-5} cm s^{-1}, which with a stem width of $a_0 = 4.55 \times 10^{-8}$ cm gives a lifetime of the terminal stem of only 1.56×10^{-3} s. Accordingly we aver that the idea that the backward reaction may be suppressed at such undercoolings by effects akin to slow desorption is worthy of consideration. In Appendix B we provide a simple semiempirical treatment showing how ϵ may vary with undercooling. This treatment gives $\epsilon \to 1$ as $\Delta T \to 0$ as required by the principle of detailed balance, which must apply at and very near T_m. It also gives very small ϵ at the undercoolings normally encountered in polymer crystallization with chain folding.

Below we calculate the flux, nucleation rate, and other quantities of interest for the flat surface model for $\Psi = 0$ with lattice strain for the case $\epsilon = 0$, i.e., non-steady-state nucleation. The case for $\epsilon = 1$ is outlined in Appendix A.

Flux and Nucleation Rate: Non-Steady-State Case ($\epsilon = 0$). The general expression[1,20] for the flux across the barrier system shown in Figure 1 is

$$S(l) = \frac{N_0A_0(A - B)}{A - B + B_1} \tag{8a}$$

which with the backward reactions suppressed reduces to

$$S(l) = N_0A_0 = N_0{}^0\beta e^{-[2b_0\sigma + a_0\sigma_s]l/kT} \tag{8b}$$

where eq 6a is employed for A_0. We have attached a superscript to β ($^0\beta$) to denote the relevant ϵ value. Here N_0 is the number of reacting species. The net rate of passage over the barrier (total flux) is defined as[1,20]

$$S_T = \frac{1}{l_u}\int_{2\sigma_e/(\Delta G_s)}^{\infty} S(l)\, dl \tag{9}$$

where l_u is the length of the basic chain unit. The lower bound of integration corresponds to the minimum possible value of l. This is readily determined by substituting $l = l_{min} = 2\sigma_e/(\Delta G_s)$ into eq 2a to find that $T_m' = T_x$, showing that a lamella of thickness l_{min} is just at the border of thermodynamic instability at its formation temperature T_x. The nucleation rate is given by[26]

$$i \equiv S_T/L = S_T/n_L a_0 \tag{10}$$

where L is the coherent substrate length. For convenience L is written as $n_L a_0$, where n_L is the number of stems of width a_0 that comprise the substrate length. As in previous treatments we let[26]

$$N_0 = C_0 n_L \tag{11}$$

which states that the number of reacting species N_0 is proportional to the number of stems on the substrate, the number C_0 being a proportionality constant that can be estimated from experiments and that is related to the configurational path degeneracy.[9] (The value of C_0 plays a significant role in determining the undercooling range occupied by regime II crystallization, a small C_0 giving a broad range.) With these developments one has the nucleation rate in events s^{-1} cm^{-1}:

$$i = {}^0\beta\frac{C_0}{a_0}\left\{\frac{kT}{(2b_0\sigma + a_0\sigma_s)l_u}\right\}e^{-4b_0[\sigma+(a_0/2b_0)\sigma_s]\sigma_e/(\Delta G_s)kT} \tag{12a}$$

$$i \cong {}^0\beta\frac{C_0}{a_0}\left\{\frac{kT}{2b_0\sigma l_u}\right\}e^{-4b_0[\sigma+\sigma_s/2]\sigma_e/(\Delta G_s)kT} \tag{12b}$$

In writing the approximate form eq 12b we have used $\sigma \gg \sigma_s$ in the preexponential factor and let $a_0 = b_0$ in the exponent. We shall use these approximations elsewhere when appropriate.

At this point it is useful to give the full expression for ${}^0\beta$ for the case of crystallization from the melt. This is conveniently given in the form[9]

$${}^0\beta = \left(\frac{{}^0\kappa}{n}\right)\left(\frac{kT}{h}\right)\left(\frac{\Delta T_s}{T_m}\right)e^{-Q_D^*/RT} \tag{13a}$$

where the numerical constant ${}^0\kappa$ in a form useful for comparisons is

$${}^0\kappa = \left(\frac{h}{kT}\right)\left[\frac{a_0(\Delta h_f)}{\sigma}\right]\left[\frac{b_0\sigma}{\zeta_0 l_f}\right]\exp(Q_D^*/RT_0) \tag{13b}$$

Here Q_D^* is the activation energy of reptation, ζ_0 the monomeric friction coefficient in the melt in erg s cm^{-2}, n the number of monomer units, l_f the length of a chain fold, and T_0 the reference temperature in the melt where ζ_0 is measured. For polyethylene ${}^0\kappa$ takes on a numerical value[9] of ~3.6.

The factor β comes from a combination of reptation theory and nucleation theory.[9] Equation 13 was derived on the basis of a model where the force associated with crystallization, which is proportional to the undercooling, draws or "reels in" a polymer chain through a reptation tube in the subcooled melt onto the substrate, this process being opposed[9,21] by the friction coefficient of the chain $\zeta_0 n$. The preexponential factors ${}^1\beta$ and ${}^1\kappa$ in the analogous expressions for the case $\epsilon = 1$ are different from those in eq 13. This arises from the following. The substrate completion rate consistent with reptation theory, g_{rept}, was calculated for a specified ζ_0 and was treated as a standard to calibrate g_{nuc}, the substrate completion rate from nucleation theory. Since g_{nuc} has somewhat different preexponential factors for the cases $\epsilon = 0$ and $\epsilon = 1$, this causes ${}^1\beta$ to differ from ${}^0\beta$ and ${}^1\kappa$ to differ from ${}^0\kappa$. The expression for g_{rept} is given in ref 9 and quoted in a footnote in Table I.

Certain modifications are required of β for crystallization from solution and for melt-crystallization at low temperatures. In the case of crystallization from dilute solution, the dissolution temperature T_d is substituted for the melting point T_m in all expressions. Further, eq 13a (or its equivalent for ${}^1\beta$) is modified by inserting an empirical factor proportional[27,28] to c^α, where c is the concentration of polymer in solution and α a factor that experiments have shown is roughly 0.3–0.5. In addition, the activation energy for transport Q_{soln}^* used should be less than Q_D^*. Last, to a zeroth approximation $n^{-1/2}$ instead of n^{-1} should be used in the expressions for β, as suggested by DiMarzio et al.[29] In high molecular weight polymers crystallizing from the melt at large undercoolings β may be written empirically[30,31] as constant × $\exp[-U^*/R(T - T_\infty)]$, where T_∞ is somewhat below the glass transition temperature T_g. It is also necessary to account at large ΔT for the diminution of the heat of fusion in ΔG according to the factor[32] T_x/T_m or $2T_x/(T_x + T_m)$.

Initial Lamellar Thickness. The initial lamellar thickness (or more precisely the length of the stems between the two fold surfaces if tilt is present) is denoted l_g^* and is determined by the flux according to the general expression[1,7,20]

$$l_g^* = \langle l \rangle = \frac{1}{l_u}\int_{2\sigma_e/\Delta G_s}^{\infty} lS(l)\, dl \Big/ \frac{1}{l_u}\int_{2\sigma_e/\Delta G_s}^{\infty} S(l)\, dl \tag{14}$$

It is found for the flat surface model where $S(l)$ is given by eq 8b for the $\epsilon = 0$ case that

$$l_g^* = \frac{2\sigma_e}{\Delta G_s} + \delta \tag{15a}$$

where for any allowable σ_s

$$\delta = \frac{kT}{2b_0\sigma + a_0\sigma_s} \cong \frac{kT}{2b_0(\sigma + \sigma_s/2)} \cong \frac{kT}{2b_0\sigma} \tag{15b}$$

In practical applications δ usually has a value of ~5 Å. The calculation for the case $\epsilon = 1$ is given in Appendix A; eq 15a is unchanged, but δ turns out to be approximately $kT/b_0\sigma$. Thus the shift from $\epsilon = 0$ to $\epsilon = 1$ does not change the form of l_g^*, but it does double δ. One easily recognizes the essential character of δ in the theory—among other properties, it prevents the unthickened lamellar crystal from melting at its formation temperature.[1]

The initial lamellar thickness has the form

$$l_g^* = \frac{C_1}{\Delta T_s} + C_2 \tag{15c}$$

This is useful in describing data on unthickened crystals.[1,23] It is ordinarily applied in the case of unstrained crystals where $\Delta T_s \to \Delta T$. As described earlier, eq 15c requires modification only at very large ΔT where the effect of $\Psi > 0$ occasionally makes itself felt. The value of C_2 found from experiments is often larger than δ because of a small temperature dependence[1] of σ_e.

Substrate Completion Rate. The general expression[1,20] for the substrate completion rate is $g \equiv a_0(A - B)$. In the $\epsilon = 0$ case where the backward reaction is suppressed, one has with eq 6c for A

$$g \equiv a_0 A = a_0\,{}^0\beta e^{-q/kT}e^{-(a_0+b_0)\sigma_s l/kT} \tag{16a}$$

Table I
Summary of Results for the Flat Surface Nucleation Model with Lattice Strain[a]

property	non-steady-state nucleation, $\epsilon = 0$ (suppressed backward reaction)	steady-state nucleation, $\epsilon = 1$ (fully active backward reaction)
1. nucleation rate i, nuclei cm^{-1} s^{-1}	$i = C_0{}^0\beta(1/a_0)\left[\frac{kT}{2b_0\sigma l_u}\right]e^{-4b_0(\sigma+\sigma_s/2)\sigma_e/(\Delta G_s)kT}$	$i = C_0{}^1\beta(1/a_0)\left[\frac{kT}{2b_0\sigma l_u}\right]\left[\frac{a_0(\Delta h_f)}{2\sigma}\right]\left(\frac{\Delta T_s}{T_m}\right)\times e^{-4b_0(\sigma+\sigma_s/2)\sigma_e/(\Delta G_s)kT}$
	$\Delta G_s = \Delta G - (a_0 + b_0)\sigma_s/a_0b_0 = (\Delta h_f)(\Delta T_s)/T_m$; $\sigma_s \ll \sigma$	ΔG_s same as for $\epsilon = 0$; $\sigma_s \ll \sigma$
2. β (events s^{-1}) and κ	${}^0\beta = \frac{{}^0\kappa}{n}\left(\frac{kT}{h}\right)\left(\frac{\Delta T_s}{T_m}\right)e^{-Q_D^*/RT}$	${}^1\beta = \frac{{}^1\kappa}{n}\left(\frac{kT}{h}\right)e^{-Q_D^*/RT}$
	${}^0\kappa = (h/kT)[a_0(\Delta h_f)/\sigma](b_0\sigma/\zeta_0 l_f)\exp(Q_D^*/RT_0) \cong 3.6$ for PE[d]	${}^1\kappa = (h/kT)(b_0\sigma/\zeta_0 l_f)\exp(Q_D^*/RT_0) \cong 0.34$ for PE[d]
3. initial lamellar thickness, cm	$l_g^* = \frac{2\sigma_e}{\Delta G_s} + \delta$ with $\delta \cong \frac{kT}{2b_0(\sigma + \sigma_s/2)} \cong \frac{kT}{2b_0\sigma}$	$l_g^* = \frac{2\sigma_e}{\Delta G_s} + \delta$ with $\delta \cong \frac{kT}{b_0(\sigma + \sigma_s/2)} \cong \frac{kT}{b_0\sigma}$
4. substrate completion rate,[b] cm s^{-1}	$g = a_0{}^0\beta e^{-q/kT}e^{-2(a_0+b_0)\sigma_s\sigma_e/(\Delta G_s)kT}$ or	$g = a_0{}^1\beta\left[\frac{a_0(\Delta h_f)}{\sigma}\right]\left(\frac{\Delta T_s}{T_m}\right)\times e^{-q/kT}e^{-2(a_0+b_0)\sigma_s\sigma_e/(\Delta G_s)kT}$ or
	$g = (g_0/n)(\Delta T_s)e^{-Q_D^*/RT}e^{-q/kT}e^{-2(a_0+b_0)\sigma_s\sigma_e/(\Delta G_s)kT}$ with $g_0 = [a_0{}^2b_0(\Delta h_f)/(\zeta_0 l_f)](1/T_m)\exp(Q_D^*/RT_0)$	$g = (g_0/n)(\Delta T_s)e^{-Q_D^*/RT}e^{-q/kT}e^{-2(a_0+b_0)\sigma_s\sigma_e/(\Delta G_s)kT}$ with g_0 same as for $\epsilon = 0$
5. growth rate in regime I, cm s^{-1}	$G_I = ({}^0Z_I/n)(\Delta T_s)e^{-Q_D^*/RT}e^{-4b_0(\sigma+\sigma_s/2)\sigma_e/(\Delta G_s)kT}$	$G_I = ({}^1Z_I/n)(\Delta T_s)e^{-Q_D^*/RT}e^{-4b_0(\sigma+\sigma_s/2)\sigma_e/(\Delta G_s)kT}$
	${}^0Z_I$ (cm s^{-1} deg^{-1}) $= C_0{}^0\kappa n_L\left(\frac{b_0kT}{h}\right)\left[\frac{kT}{2b_0\sigma l_u}\right](1/T_m)$	${}^1Z_I$ (cm s^{-1} deg^{-1}) $= C_0{}^1\kappa n_L\left(\frac{b_0kT}{h}\right)\times\left[\frac{a_0(\Delta h_f)}{2\sigma}\right]\left[\frac{kT}{2b_0\sigma l_u}\right](1/T_m)$
6. growth rate in regime II, cm s^{-1}	$G_{II} = ({}^0Z_{II}/n)(\Delta T_s)e^{-Q_D^*/RT}e^{-2b_0(\sigma+1.5\sigma_s)\sigma_e/(\Delta G_s)kT}$	$G_{II} = ({}^1Z_{II}/n)(\Delta T_s)e^{-Q_D^*/RT}e^{-2b_0(\sigma+1.5\sigma_s)\sigma_e/(\Delta G_s)kT}$
	${}^0Z_{II}$ (cm s^{-1} deg^{-1}) $= (C_0{}^{1/2})\,{}^0\kappa\left(\frac{b_0kT}{h}\right)\left(\frac{kT}{b_0\sigma l_u}\right)^{1/2}\times(1/T_m)e^{-q/2kT}$	${}^1Z_{II}$ (cm s^{-1} deg^{-1}) $= (C_0{}^{1/2})\,{}^1\kappa\left(\frac{b_0kT}{h}\right)\times\left[\frac{a_0(\Delta h_f)}{\sigma T_m}\right]\left(\frac{kT}{2b_0\sigma l_u}\right)^{1/2}e^{-q/2kT}$
7. growth rate in regime III,[c] cm s^{-1}	$G_{III} = ({}^0Z_{III}/n)(\Delta T_s)e^{-Q_D^*/RT}e^{-4b_0(\sigma+\sigma_s/2)\sigma_e/(\Delta G_s)kT}$	$G_{III} = ({}^1Z_{III}/n)(\Delta T_s)e^{-Q_D^*/RT}e^{-4b_0(\sigma+\sigma_s/2)\sigma_e/(\Delta G_s)kT}$
	${}^0Z_{III}$ (cm s^{-1} deg^{-1}) $= \frac{C_0{}^0\kappa n_L'}{K_{corr}}\left(\frac{b_0kT}{h}\right)\left[\frac{kT}{2b_0\sigma l_u}\right](1/T_m)$	${}^1Z_{III}$ (cm s^{-1} deg^{-1}) $= \frac{C_0{}^1\kappa n_L'}{K_{corr}}\left(\frac{b_0kT}{h}\right)\times\left[\frac{a_0(\Delta h_f)}{2\sigma}\right]\left[\frac{kT}{2b_0\sigma l_u}\right](1/T_m)$

[a] The definitions of all quantities are given in the text, as are the approximations employed. The expressions given here apply to crystallization from the melt at normal undercoolings. Adaption to crystallization at low melt-crystallization temperatures or from solution is indicated in the text. The value of K_{corr} near the II → III regime transition is ~4.47.[10] To simplify a number of the exponents, $(a_0/2b_0)\sigma_s$ has been approximated as $\sigma_s/2$. [b] The expression for g_{rept} on which g_0 is based is eq 13 of ref 9: β is calibrated in the absence of strain. The expression for g_{rept} is $(1/n)[a_0{}^2b_0(\Delta h_f)\exp(Q_D^*/RT_0)/\zeta_0 l_f](\Delta T/T_m)\exp(-Q_D^*/RT)\exp(-q/kT)$. [c] The predicted n^{-1} behavior will likely not persist deep in regime III. [d] Reference 9. PE = polyethylene.

Substituting l_g^* as given by eq 15a and 15b for l above, one obtains

$$g = a_0{}^0\beta e^{-q/kT}e^{-2(a_0+b_0)\sigma_s\sigma_e/(\Delta G_s)kT}e^{-(\sigma_s/\sigma)[(a_0+b_0)/2b_0]}$$

$$g \cong a_0{}^0\beta e^{-q/kT}e^{-2(a_0+b_0)\sigma_s\sigma_e/(\Delta G_s)kT} \cong a_0{}^0\beta e^{-q/kT}e^{-4b_0\sigma_s\sigma_e/(\Delta G_s)kT} \quad (16b)$$

The form of eq 16b where ${}^0\beta$ is given explicitly is shown in Table I. The expression for g based on $\epsilon = 1$ is developed in Appendix A and given in Table I. It differs but little from that based on $\epsilon = 0$.

Observe from eq 16b that lattice strain as measured by σ_s can considerably reduce the substrate completion rate. This effect is augmented by the fact that $\Delta G_s < \Delta G$. The substrate completion rate for the serrated surface model discussed below exhibits a similar effect, which will prove useful in explaining the curved edge of the 200 sector of certain polyethylene single crystals.

(C) Growth Rates in Regimes I, II, and III. In calculating G_I, G_{II}, and G_{III} for the flat surface model with lattice strain for the case $\epsilon = 0$ representing non-steady-state nucleation, we employ eq 12b for i and 16b for g. We consider first regime I, which occurs at low undercoolings, where[21,33,34]

$$G_I \equiv b_0 iL \approx b_0 in_L a_0 \quad (17)$$

Here the nucleation rate is quite low, and one nucleus, deposited at a random position, causes the completion of a new layer of thickness b_0 on the substrate of length L. We interpret L as the mean distance between defects that terminate substrate completion.[9] The resultant expression for G_I is given in Table I.

A recent treatment[9] has revealed that the magnitude of L for the 110 face of melt-crystallized polyethylene is

considerably smaller than had been previously supposed. The correct value of L is within a factor of about 2 or 3 of 210 Å; it could easily be 500 Å. The new value eliminates certain difficulties associated with the earlier estimates.[9] The magnitude of L is unaffected by the choice of ϵ.

Regime II crystallization (multiple nucleation on the substrate) occurs at temperatures below regime I (if regime I occurs at all) and is quite common. The observable growth rate in regime II is defined as[21,33,34]

$$G_{II} \equiv b_0(2ig)^{1/2} \tag{18}$$

Here the growth rate is proportional to $i^{1/2}$ rather than i as in regime I. The result is listed in Table I.

At sufficiently large undercoolings the surface nucleation rate becomes extremely high and the mean separation ("niche separation") between the numerous nuclei assumes a value close to that of a few molecular widths. Thus, primary nucleation once again dominates the growth rate.[35] (The "niche separation" between the nuclei is approximately proportional to $(2g/i)^{1/2}$; as shown by Guttman and DiMarzio[10] this simple formula needs correction in the vicinity of the regime II → III transition, which leads to the numerical factor $K_{corr} \cong 4.47$ in the formulas for G_{III} given in Table I. At high temperatures in regime II, the niche separation formula becomes increasingly accurate.) Under these circumstances, regime III is entered and the growth rate once again becomes directly proportional to the nucleation rate i. Specifically[35]

$$G_{III} \equiv b_0 i n_L' a_0 \tag{19}$$

where $n_L' \sim 1$ to, say, 2. The resultant formula for the case $\epsilon = 0$ is given in Table I.

Corresponding expressions for G_I, G_{II}, and G_{III} based on the assumption $\epsilon = 1$ are also given Table I. In deriving these expressions, eq A7 of Appendix A was used for i, and eq A16 or A17 for g.

(D) Summary Remarks: Flat Surface Nucleation Model. The flat surface nucleation model with lattice strain yields expressions for the growth rates in regimes I, II, and III that strongly resemble those commonly employed in the analysis of data (see Table I). In simplified form, the growth rates may be written

$$G = G_0(\Delta T_s)e^{-Q_D^*/RT}e^{-K_g/T(\Delta T_s)} \tag{20a}$$

where

$$K_g = K_{g(I)} = K_{g(III)} \cong 4b_0(\sigma + \sigma_s/2)\sigma_e T_m/(\Delta h_f)k \tag{20b}$$

$$K_g = K_{g(II)} \cong 2b_0(\sigma + 1.5\sigma_s)\sigma_e T_m/(\Delta h_f)k \tag{20c}$$

For vanishingly small σ_s, these expressions lead to the standard forms for G and K_g for a specified regime. The largest effect of a small σ_s, say 0.5 erg cm^{-2}, would be the reduction in the undercooling from ΔT to ΔT_s as described by eq 2b. The change in K_g itself could hardly be detected because σ is so much larger than σ_s. In this sense, the effect of lattice strain in the flat surface model is essentially unremarkable. Equations 20 hold independent of whether $\epsilon = 1$ or $\epsilon = 0$ is employed in the derivation. They therefore have a quite general basis. It remains to be said that expressions of the form of eq 20 in the limit $\sigma_s \to 0$ have found wide and successful application. It should be recalled that $\exp(-Q_D^*/RT)$ is to be replaced by $\exp[-U^*/R(T - T_\infty)]$ in applications at low crystallization temperatures.

In Table I we show G_0 for a sharp fraction crystallizing from the melt to vary as Z/n, the factor n^{-1} arising directly from reptation in the melt. A more precise formulation that accounts for the free energy of attachment of the first chain gives $Z_I/n^{4/3}$ for regime I and $Z_{II}/n^{7/6}$ for regime II for sharp fractions.[9] Fractions with a significant low molecular weight component tend to follow Z/n^a, where a is 0.5–0.7.[9] We have definite reservations concerning the $G_{III} \propto n^{-1}$ prediction seen in Table I if the crystallization takes place deep in regime III. Here only reptation of "slack" may occur,[9,36] causing a considerably muted variation with n; there are no experiments known to us that bear on this issue. A similar falloff in the dependence on n is to be expected at very high molecular weights where the "reeling in" process for a typical molecule will be seriously perturbed by numerous acts of multiple nucleation.[9]

Table II
Comparison of Properties for $\epsilon = 0$ and $\epsilon = 1$ for the Flat Surface Model[a]

property, p_ϵ	ratio $p_{\epsilon=0}/p_{\epsilon=1}$
i	2
β	$[a_0(\Delta h_f)/\sigma][\Delta T_s/T_m]$
κ	$a_0(\Delta h_f)/\sigma$
l_g^*	slightly less than unity because of difference in δ
δ in $l_g^* = (2\sigma_e/\Delta G_s) + \delta$	1/2
g	1
G_I, Z_I	2
G_{II}, Z_{II}	$2^{1/2}$
G_{III}, Z_{III}	2

[a] Calculated for the case where the friction coefficient ζ_0 is fixed. Such quantities as a_0, b_0, Δh_f, T_m, σ, σ_e, σ_s, and Q_D^* are also assumed to be the same for the $\epsilon = 0$ and $\epsilon = 1$ formulas in Table I.

Now that the properties of the flat surface model with lattice strain included are known, it is possible to state that we are aware of no experimental data for the rate of growth of a dominant growth front that has been treated by using this model that need to be corrected for the effect of σ_s. An indication of the phenomena that might invite such a correction is the following. The appropriate undercooling to employ in making plots of ln G − ln ("ΔT") + Q_D^*/RT vs $1/T$("ΔT") is obviously "ΔT" = $\Delta T_s = T_s - T_x$ and not "ΔT" = T_m (or T_d) − T_x if a significant σ_s contribution is present. Use of T_m (or T_d) − T_x in such situations will lead to curvature for the plots in a given regime. If such curvature is found, it may be taken as an indication that lattice strain may be lowering the effective melting point from T_m (or T_d) to T_s. The 110 sector of polyethylene exhibits no such effects and conforms well to the flat surface model with $\sigma_s = 0$ (see ref 1 and 9 and the discussion in section IV).

The substrate completion rate is affected by a finite σ_s, as given by $g \propto \exp[-2(a_0 + b_0)\sigma_s\sigma_e/(\Delta G_s)kT]$ in eq 16b. However, for the flat surface model this has little effect on the overall growth rate, since the contribution of σ is much larger as the K_g formulas above show. In contrast, the serrated surface model to be discussed shortly has a "K_g" that is completely dominated by the product $\sigma_s\sigma_e$ rather than $(\sigma + \sigma_s/2)\sigma_e$ or $(\sigma + 1.5\sigma_s)\sigma_e$ as in the flat surface model.

Note that the form of the formula for l_g^* for the flat surface model is unaffected in form by the presence of a finite σ_s. However, a new undercooling scale based on T_s rather than T_m enters the picture when σ_s in introduced.

Finally it is of interest to compare the results of the properties associated with the flat surface model as calculated on the basis $\epsilon = 0$ (non-steady-state nucleation, inactive backward reaction) and $\epsilon = 1$ (steady-state nucleation, active backward reaction). This can done by inspection of Table I. However, this comparison is most conveniently effected in Table II. Recall that the

Table III
Summary of Results for the Serrated Edge Model with Lattice Strain[a]

property	non-steady-state nucleation, $\epsilon = 0$ (suppressed backward reaction)	steady-state nucleation, $\epsilon = 1$ (fully active backward reaction)[b]
1. nucleation rate i (nuclei cm^{-1} s^{-1}); also ΔG_s and ΔT_s	$i = C_0{}^0\beta(1/a_0)\left[\frac{kT}{2(2^{1/2})b_0\sigma_s l_u}\right]e^{-4(2^{1/2})b_0\sigma_s\sigma_e/(\Delta G_s)kT}$	$i = C_0{}^1\beta(1/a_0)\left[\frac{kT}{2(2^{1/2})b_0\sigma_s l_u}\right]\left[\frac{a_0(\Delta h_f)}{2(2^{1/2})\sigma_s}\right]\times \left[\frac{\Delta T_s}{T_m}\right]e^{-4(2^{1/2})b_0\sigma_s\sigma_e/(\Delta G_s)kT}$
	$\Delta G_s = \Delta G - 2^{1/2}\sigma_s/b_0 = (\Delta h_f)(\Delta T_s)/T_m$	ΔG_s and ΔT_s same as for $\epsilon = 0$
	$\Delta T_s = T_s - T_x = T_m\left[1 - \frac{2^{1/2}\sigma_s}{b_0(\Delta h_f)}\right] - T_x$	
2. β (events s^{-1}) and κ	${}^0\beta = \frac{{}^0\kappa}{n}\left(\frac{kT}{h}\right)\left(\frac{\Delta T_s}{T_m}\right)e^{-Q_D^*/RT}$	${}^1\beta = \frac{{}^1\kappa}{n}\left(\frac{kT}{h}\right)\left(\frac{\Delta T_s}{T_m}\right)e^{-Q_D^*/RT}$
	${}^0\kappa = (h/kT)e\left[\frac{a_0(\Delta h_f)}{2^{1/2}\sigma_s}\right]\left[\frac{2^{1/2}b_0\sigma_s}{\zeta_0 l_f}\right]\times \exp(Q_D^*/RT_0)$	${}^1\kappa = (h/kT)e^2\left[\frac{a_0(\Delta h_f)}{2^{1/2}\sigma_s}\right]\left[\frac{2^{1/2}b_0\sigma_s}{\zeta_0 l_f}\right]\times \exp(Q_D^*/RT_0)$
3. initial lamellar thickness, cm	$l_g^* = \frac{2\sigma_s}{\Delta G_s} + \delta$ with $\delta = \frac{kT}{2(2^{1/2})b_0\sigma_s}$	$l_g^* = \frac{2\sigma_s}{\Delta G_s} + \delta$ with $\delta \cong \frac{kT}{2^{1/2}b_0\sigma_s}$
4. substrate completion rate, cm s^{-1}	$g = a_0{}^0\beta(1/e)e^{-q/kT}e^{-4(2^{1/2})b_0\sigma_s\sigma_e/(\Delta G_s)kT}$ or $g = (g_0/n)(\Delta T_s)e^{-Q_D^*/RT}e^{-q/kT}e^{-4(2^{1/2})b_0\sigma_s\sigma_e/(\Delta G_s)kT}$ with $g_0 = \frac{a_0{}^2b_0(\Delta h_f)}{\zeta_0 l_f T_m}\exp(Q_D^*/RT_0)$	$g = a_0{}^1\beta(1/e^2)e^{-q/kT}e^{-4(2^{1/2})b_0\sigma_s\sigma_e/(\Delta G_s)kT}$ or $g = (g_0/n)(\Delta T_s)e^{-Q_D^*/RT}e^{-q/kT}e^{-4(2^{1/2})b_0\sigma_s\sigma_e/(\Delta G_s)kT}$ with g_0 same as for $\epsilon = 0$
5. growth rate in regime I, cm s^{-1}	$G_I = ({}^0Z_I/n)(\Delta T_s)e^{-Q_D^*/RT}e^{-4(2^{1/2})b_0\sigma_s\sigma_e/(\Delta G_s)kT}$ ${}^0Z_I = C_0{}^0\kappa n_L\left[\frac{b_0kT}{h}\right]\left[\frac{kT}{2(2^{1/2})b_0\sigma_s l_u}\right](1/T_m)$	$G_{II} = ({}^1Z_I/n)(\Delta T_s)^2e^{-Q_D^*/RT}e^{-4(2^{1/2})b_0\sigma_s\sigma_e/(\Delta G_s)kT}$ ${}^1Z_I = C_0{}^1\kappa n_L\left[\frac{b_0kT}{h}\right]\left[\frac{a_0(\Delta h_f)}{2(2^{1/2})\sigma_s}\right]\times \left[\frac{kT}{2(2^{1/2})b_0\sigma_s l_u}\right](1/T_m)^2$
6. growth rate in regime II,[c] cm s^{-1}	$G_{II} = ({}^0Z_{II}/n)(\Delta T_s)e^{-Q_D^*/RT}e^{-4(2^{1/2})b_0\sigma_s\sigma_e/(\Delta G_s)kT}$ ${}^0Z_{II} = \frac{(C_0{}^{1/2})^0\kappa}{e^{1/2}}\left(\frac{b_0kT}{h}\right)\left(\frac{kT}{2^{1/2}b_0\sigma_s l_u}\right)^{1/2}\times (1/T_m)e^{-q/2kT}$	$G_{II} = ({}^1Z_{II}/n)(\Delta T_s)^{3/2}e^{-Q_D^*/RT}e^{-4(2^{1/2})b_0\sigma_s\sigma_e/(\Delta G_s)kT}$ ${}^1Z_{II} = \frac{(C_0{}^{1/2})^1\kappa}{e}\left[\frac{b_0kT}{h}\right]\left[\frac{a_0(\Delta h_f)}{2^{1/2}\sigma_s}\right]^{1/2}\times \left[\frac{kT}{2(2^{1/2})b_0\sigma_s l_u}\right]^{1/2}(1/T_m)^{3/2}e^{-q/2kT}$
7. growth rate in regime III, cm s^{-1}	$G_{III} = ({}^0Z_{III}/n)(\Delta T_s)e^{-Q_D^*/RT}e^{-4(2^{1/2})b_0\sigma_s\sigma_e/(\Delta G_s)kT}$ ${}^0Z_{III} = \frac{C_0{}^0\kappa n_L'}{K_{corr}}\left[\frac{b_0kT}{h}\right]\left[\frac{kT}{2(2^{1/2})b_0\sigma_s l_u}\right](1/T_m)$	$G_{III} = ({}^1Z_{III}/n)(\Delta T_s)^2e^{-Q_D^*/RT}e^{-4(2^{1/2})b_0\sigma_s\sigma_e/(\Delta G_s)kT}$ ${}^1Z_{III} = \frac{C_0{}^1\kappa n_L'}{K_{corr}}\left[\frac{b_0kT}{h}\right]\left[\frac{a_0(\Delta h_f)}{2(2^{1/2})\sigma_s}\right]\times \left[\frac{kT}{2(2^{1/2})b_0\sigma_s l_u}\right](1/T_m)^2$

[a] The results given hold for the "square" model depicted in Figure 2 where $a_0 = 2b_0$. This is a good approximation when $a_0 \approx 2b_0$. The factor $2^{1/2}$ becomes $5^{1/2}/2$ when $a_0 = b_0$. The prefactors ${}^0Z_I$, ${}^0Z_{II}$, ${}^0Z_{III}$ are in cm s^{-1} deg^{-1}. The prefactors ${}^1Z_I$ and ${}^1Z_{III}$ are in cm s deg^{-2}, and ${}^1Z_{II}$ is in cm s^{-1} deg$^{-3/2}$. [b] A factor $[1 - \exp(-a_0b_0\delta\Delta G_s/kT]$ appears in the derivation for g for the case $\epsilon = 1$. Because σ_s is small, δ is large; accordingly this factor is essentially unity at normal undercoolings and this table reflects this approximation. [c] Experiments are expected to correspond to regime II.

matching point is that g_{rept} has been set as the standard, and g_{nuc} for $\epsilon = 0$ and $\epsilon = 1$ set equal to this quantity.[9] Therefore, the absolute value of $g_{nuc}(\epsilon=0)$ is the same as $g_{nuc}(\epsilon=1)$, so that for g, $p_{\epsilon=0}/p_{\epsilon=1} \equiv 1$. It is readily seen that the differences are minimal, showing that the forward reactions dominate all properties such as G_I, G_{II}, G_{III}, and l_g^* that depend on the flux across the nucleation barrier.

III. Nucleation on a Nonideal Serrated Surface

The serrated surface model is depicted in Figure 2. Note that the serration is *on a molecular level*. We shall follow the procedures devised for treating the flat surface model in essentially the same sequence, with both the $\epsilon = 1$ and $\epsilon = 0$ results being summarized in Table III. We begin with a discussion of the thermodynamic behavior induced by the effect of σ_s as a prelude to constructing $\Delta\phi_\nu$ and thence the rate constants. The origin of the lattice strain is the same as in the case of the flat surface model, i.e., it is caused by repulsions of chain folds that cause a general expansion of the lattice. To highlight the special

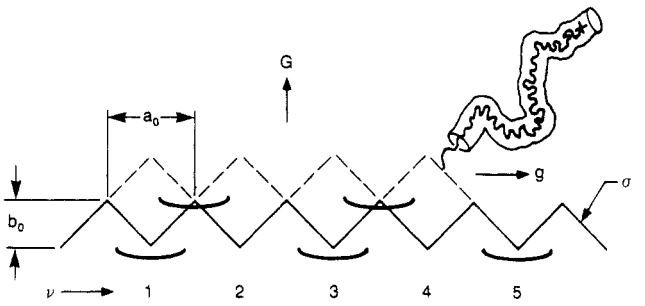

Figure 2. Model for nucleation and substrate completion on a nonideal serrated surface. Note that the serration is on a molecular level. The first ($\nu = 1$) stem is put down at a cost in free energy of $2(2^{1/2})b_0\sigma_s l$ where $\sigma_s < \sigma$. Note that for a stem with a square cross section $a_0 = 2b_0$. Each stem added to the substrate after the first incurs a free energy cost $q_{fold} + 2(2^{1/2})b_0\sigma_s l$, where σ_s represents the nonideality of the substrate.

properties of the model, we treat the limiting case where there is no term in σ whatsoever.

Thermodynamics of Bulk and Surface States. It is necessary to emphasize at the outset that because of the different geometry of the chains on the serrated surface, ΔG_s, T_m', ΔT_s, and T_s differ from those for the flat surface model. (Note the definitions of a_0 and b_0 in Figure 2.) For simplicity, we take the stem to be square and note that then $a_0 = 2b_0$. Observe that b_0 plays the role of a layer thickness. The lattice strain energy is calculated as $2(2^{1/2})b_0\sigma_s l$ divided by $2b_0{}^2 l = 2^{1/2}\sigma_s/b_0$, which is also equal to $2(2^{1/2})\sigma_s/a_0$. This is essentially the "buried" interfacial surface free energy divided by the volume of a stem and as before has the units of free energy per unit volume. As each stem is added to the surface during substrate completion, it incurs an interfacial energy of $2^{1/2}b_0\sigma_s l$ for each of the sides in contact with the substrate because of the strain in the substrate; by this accounting a "buried" stem experiences a σ_s effect totalling $2(2^{1/2})b_0\sigma_s l$ or $2^{1/2}a_0\sigma_s l$. A "buried" stem experiences a σ_s effect on all four of its sides, but its particular share is the σ_s effect associated with the two of its sides that fitted onto the surface during its addition to the substrate. Then

$$\Delta G_s = \Delta G - 2^{1/2}\sigma_s/b_0 = (\Delta h_f)(\Delta T_s)/T_m \quad (21a)$$

where $\Delta G = (\Delta h_f)(\Delta T)/T_m$ with $\Delta T = T_m - T_x$ and where $\Delta T_s = T_s - T_x$. Also

$$T_m' = T_m\left\{1 - \frac{2\sigma_e}{(\Delta h_f)l} - \frac{2^{1/2}\sigma_s}{(\Delta h_f)b_0}\right\} \quad (21b)$$

which is the analogue of eq 2a. Further

$$\Delta T_s = T_s - T_x = T_m\left[1 - \frac{2^{1/2}\sigma_s}{(\Delta h_f)b_0}\right] - T_x \quad (21c)$$

which is the analogue of eq 2b. The quantity $T_m[1 - 2^{1/2}\sigma_s/(\Delta h_f)b_0]$ is T_s. In the above expressions the factor $2^{1/2}\sigma_s/b_0$ may be replaced by $2(2^{1/2})\sigma_s/a_0$. The foregoing expressions may readily be generalized[6] to account for situations where a_0 is not exactly equal to $2b_0$, i.e., where the cross section of the stem is not exactly square. Recall also that σ_s represents an average value of the interfacial surface free energy and may vary slightly with the lamellar thickness.

The surface nucleus forms according to

$$\Delta\phi_\nu = 2(2^{1/2})\nu b_0\sigma_s l + 2(\nu - 1)a_0b_0\sigma_e - \nu a_0b_0 l(\Delta G) \quad (22a)$$

This rearranges to

$$\Delta\phi_\nu = 2(2^{1/2})b_0\sigma_s l - a_0b_0 l(\Delta G) - (\nu - 1)a_0b_0\{l[(\Delta G) - 2^{1/2}\sigma_s/b_0] - 2\sigma_e\} \quad (22b)$$

As before a_0b_0 is the cross-sectional area of the chain, σ_e the mean fold free energy, and ν the number of stems added to the substrate. The mean work of chain folding is given by $q = 2a_0b_0\sigma_e$. Note the absence of a lateral surface free energy term analogous to $2b_0\sigma l$ of the flat surface model (cf. eq 3b).

The ideal serrated surface model has $\sigma_s = 0$, which means that there is no nucleation barrier for the first stem. (Strictly speaking the attachment of the first stem involves a free energy barrier[9] $\lambda kT \ln (l_0/x_0)$, but we omit this as in the flat surface model.) In the serrated surface model treated below, the first and all other stems experience a σ_s effect because of the nonideal nature of the substrate, which can be traced back to the expansion of the lattice resulting from repulsion of chain folds.

General and Practical Rate Constants. The general rate constants are constructed in the same manner as those for the flat surface model, i.e., by initially assuming detailed balance and conformity to $\Delta\phi_\nu$. Thus

$$A_0 = \beta e^{-2(2^{1/2})b_0\sigma_s l/kT} e^{\Psi[a_0b_0(\Delta G_s) + 2(2^{1/2})b_0\sigma_s]l/kT} \quad (23a)$$

$$B = B_1 = \beta e^{-(1-\Psi)[a_0b_0l(\Delta G_s) + 2(2^{1/2})b_0\sigma_s]l/kT} \quad (23b)$$

$$A = \beta e^{-q/kT} e^{-2(2^{1/2})b_0\sigma_s l/kT} e^{\Psi[a_0b_0(\Delta G_s) + 2(2^{1/2})b_0\sigma_s]l/kT} \quad (23c)$$

When compared with eq 22b, the ratios A_0/B_1 and A/B show that detailed balance holds.

From eq 23a one finds

$$(\Delta T_s)_c = \frac{2(2^{1/2})\sigma_s T_m}{a_0(\Delta h_f)} \frac{(1 - \Psi)}{\Psi} \quad (24)$$

as the critical undercooling as measured from T_s for the occurrence of a δ catastrophe. This is the counterpart of eq 5. Mostly because $\sigma_s < \sigma$, $(\Delta T_s)_c$ is smaller for the serrated model than it is for the flat surface model. For the nominal values introduced previously for illustrative purposes ($\sigma_s = 1.5$ erg cm^{-2}, $T_m = 420$ K, $a_0 = 5 \times 10^{-8}$ cm, and $\Delta h_f = 2.5 \times 10^9$ erg cm^{-3}) one gets $(\Delta T_s)_c = 28.5$ °C for $\Psi = {}^1/_3$ and 57.0 °C for $\Psi = {}^1/_5$.

As before we employ the $\Psi = 0$ approximation, implying a "partial stem" character to the activated state, and introduce ϵ to obtain the practical rate expressions

$$A_0 = \beta e^{-2(2^{1/2})b_0\sigma_s l/kT} \quad (25a)$$

$$B_1 = B = \epsilon\beta e^{-[a_0b_0l(\Delta G_s) + 2(2^{1/2})b_0\sigma_s]l/kT} \quad (25b)$$

$$A = \beta e^{-q/kT} e^{-2(2^{1/2})b_0\sigma_s l/kT} \quad (25c)$$

Below we outline the calculation of i, $l_g{}^*$, and g, and thence G_I, G_{II}, G_{III} for the case $\epsilon = 0$, corresponding to a muted backward reaction such that the stem has a sticking coefficient of unity (non-steady-state nucleation).

Nucleation Rate, Initial Lamellar Thickness, and Substrate Completion Rate. The flux for the nonideal serrated edge model with $\epsilon = 0$ is

$$S(l) = N_0A_0 = C_0n_L{}^0\beta e^{-2(2^{1/2})b_0\sigma_s l/kT} \quad (26)$$

giving the total flux, S_T, according to eq 9 and thence the nucleation rate

$$i = S_T/n_La_0 = {}^0\beta\left(\frac{C_0}{a_0}\right)\left(\frac{kT}{2(2^{1/2})b_0\sigma_s l_u}\right)e^{-4(2^{1/2})b_0\sigma_s\sigma_e/(\Delta G_s)kT} \quad (27)$$

Here ΔG_s is defined as in eq 21a. Because of the factor $\sigma_s{}^{-1}$ in the preexponential in this limiting case of the model, eq 27 is valid only for finite σ_s. From eq 14 and 26 the initial lamellar thickness is found to be

$$l_g^* = \frac{2\sigma_e}{\Delta G_s} + \delta = \frac{2\sigma_e}{\Delta G_s} + \frac{kT}{2(2^{1/2})b_0\sigma_s} \quad (28)$$

which is valid only for finite σ_s. The substrate completion rate is

$$g \equiv a_0 A = a_0{}^0\beta e^{-q/kT} e^{-2(2^{1/2})b_0\sigma_s l/kT} \quad (29a)$$

or

$$g = a_0{}^0\beta(1/e)e^{-q/kT} e^{-4(2^{1/2})b_0\sigma_s\sigma_e/(\Delta G_s)kT} \quad (29b)$$

where eq 28 has been used for l. Expressions for ${}^0\beta$ and ${}^0\kappa$ are given in Table III.

Because of the nearly identical dependence of i and g on undercooling, the expressions for G for all three crystallization regimes are similar in form. For regimes I and III one has with $G_I \equiv b_0 i n_L a_0$ and $G_{III} \equiv b_0 i n_L' a_0$ the expression

$$G_{I\text{ or }III} = (Z_{I\text{ or }III}/n)(\Delta T_s)e^{-Q_D^*/RT} e^{-K_s/T(\Delta T_s)} \quad (30a)$$

and for regime II with $G_{II} \equiv b_0(2ig)^{1/2}$

$$G_{II} = (Z_{II}/n)(\Delta T_s)e^{-Q_D^*/RT} e^{-K_s/T(\Delta T_s)} \quad (30b)$$

For all three regimes the nucleation exponent is

$$K_s = \frac{4(2^{1/2})b_0\sigma_s\sigma_e T_m}{\Delta h_f k} \quad (30c)$$

To highlight an important property of the serrated surface model, we rewrite the substrate completion rate in eq 29b in the form

$$g = (g_0/n)(\Delta T_s)e^{-q/kT} e^{-Q_D^*/RT} e^{-K_s/T(\Delta T_s)} \quad (30d)$$

Thus, since $\exp(-q/kT)$ is a comparatively slowly varying function of temperature, the model has it that *the growth rate and the substrate completion rate for finite σ_s are nearly identical as regards their variation with temperature and undercooling.* Note that g is considerably reduced by σ_s.

Another striking feature of the model is that there are no changes of slope at any regime transitions in a plot of $\ln G - \ln(\Delta T_s) + Q_D^*/RT$ vs $1/T(\Delta T_s)$ or one of the common variants of such a plot (such as the commonly employed one that omits the $\ln(\Delta T_s)$ term). Only the Z value is substantially different for the three regimes (see Table III). The high nucleation rate relative to the substrate completion rate clearly implies that multiple nucleation will occur so that one anticipates that the preexponential factor Z will correspond to regime II or possibly regime III, irrespective of any regime transitions that may occur on the unstrained growth front of an adjoining sector. (Note that if the front under consideration is definitely curved, regime I is inappropriate at the outset.) The adaptation to dilute solution is the same as described for the flat surface model.

Table III collects the results for the serrated surface model in a form convenient for comparing the $\epsilon = 0$ case (non-steady-state nucleation) with the $\epsilon = 1$ case (steady-state nucleation). The method for deriving the results for $\epsilon = 1$ in Table III parallel those employed in Appendix A for the flat surface model. As in the case of the flat surface model, there are no essential differences in form. As Table III shows, only the preexponential factors are different for i, g, G_I, G_{II}, and G_{III}. The most notable quantitative difference is in δ, which is quite large in the $\epsilon = 1$ case. Because we have treated the limiting case of the serrated model with no σ effect whatsoever, the flux-dependent properties (i.e., i, δ, G_I, G_{II}, G_{III}) in Table III are valid only for finite σ_s. By introducing a minimal degree of flat surface character into the model by inserting a term $2y_0\sigma l$ for the first stem in eq 22b, where y_0 is a small vertical distance ("blunted corner") associated with a σ-type surface, the infinities in i and δ are avoided even when $\sigma_s \to 0$. For example, δ in eq 28 then becomes $kT/(2(2^{1/2})b_0\sigma_s + 2y_0\sigma)$. The unique properties of the serrated model as given by eq 30 are still retained with this modification for a wide range of σ_s values provided that $y_0\sigma$ is rather smaller than $b_0\sigma_s$. Equation 30 holds irrespective of whether $\epsilon = 0$ or $\epsilon = 1$ (Table III).

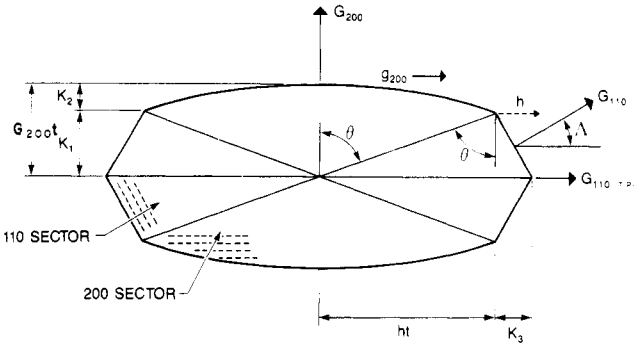

Figure 3. Polyethylene single crystal with curved 200-type edge (schematic). Dashed lines symbolize folds.

In the serrated surface model with chains possessing a square cross section such that $a_0 = 2b_0$ as depicted in Figure 2, the nearest point of "adjacent" reentry during substrate completion is actually a rather distant second-nearest neighbor. In this version of the model, the interaction between two adjacent stems on the substrate would be quite weak. In the version of the model where the shape of the molecular cross section is adjusted so that $a_0 \approx b_0$ (which corresponds more closely, for instance, to the 200 front in polyethylene) the interactions between adjacent stems on the substrate are somewhat more like those occurring between normal nearest neighbors. In this case the concept of adjacent reentry takes on something closer to its customary meaning. For the limiting version of the serrated surface model presented here, which has no term in σ, one might expect a reduced degree of "tight" folding. This is because there is no energetically favored niche on the adjacent site as there is in the flat surface model. If the modification of the serrated model with a small degree of flat surface character with a term in $2y_0\sigma_s l$ is invoked, there would be a corresponding energetic advantage for adjacent reentry in the substrate completion process.

The serrated surface model is clearly indicated as applicable if an analysis of growth rate and other data shows that the substrate completion rate and the growth rate of the face under consideration have essentially identical dependences on temperature according to eq 30. The curved 200-type face of polyethylene single crystals exhibits precisely this behavior when g_{200} and G_{200} are extracted from the growth rate and crystal shape data of Organ and Keller by using the method of analysis devised by Mansfield[4] to obtain g_{200}. In the following, we outline the treatment of certain of the data of Organ and Keller to illustrate how curved edges arise.

IV. Reduced Substrate Completion Rates and Curved Edges: The Mansfield Equations for Growth of a Crystal with Two Types of Sectors

It is useful to show how a substrate completion rate that has been reduced by the effect of lattice strain can lead directly to a curved edge. The system we have in mind is depicted in Figure 3, which shows a somewhat idealized version of a polyethylene single crystal with both 110- and

200-type sectors. This sketch draws heavily on the findings of Wittmann and Lotz.[37] Khoury and Bolz[38] have shown that the chains in the 200-type sectors exhibit tilt and that this tilt is variable; we take this to be consistent with the presence of lattice strain.

The edgewise rate of advance of the 200-type sector is the velocity h, which is controlled in part by G_{110}, the growth rate of the 110 face. Thus one has a substrate for the 200-type face that involves steadily moving boundary conditions. The rate of advance of the 110 face is assumed to be of the normal type, i.e., it is treated in terms of the flat surface model where the expressions given by eq 20 for $\sigma_s \cong 0$ hold for both regimes I and II with $K_{g(I)} \cong 2K_{g(II)}$ (cf. Table I). The differential equations relevant to the 200-type face are those of Frank:[33]

$$\frac{\partial \mathcal{R}}{\partial t} + g\frac{\partial \mathcal{R}}{\partial x} = -2g\mathcal{R}\mathcal{L} + i \tag{31a}$$

$$\frac{\partial \mathcal{L}}{\partial t} - g\frac{\partial \mathcal{L}}{\partial x} = -2g\mathcal{R}\mathcal{L} + i \tag{31b}$$

which are to be solved in the moving interval $-ht < x < ht$ for $2h$, the relative velocity of the two boundaries of the growing 200 sector. The velocity h is determined by both the growth of the adjoining 110 sector and the advance of the 200 sector according to $h = (G_{110}/\cos \Lambda) - G_{200} \tan \Lambda[1 - (h/g_{200})^2]^{1/2}$, where the angle Λ is set by the unit cell dimensions, a and b: $\Lambda = \tan^{-1}(a/b) = 32.9°$. The functions $\mathcal{R}(x,t)$ and $\mathcal{L}(x,t)$ are the concentrations of right and left moving steps on the 200 growth front. The quantity $i = i_{200}$ is the nucleation rate, and $g = g_{200}$ is the substrate completion rate on the 200-type face.

When carried out in the context of the geometry given in Figure 3, the solutions of the above equations have been shown by Mansfield to lead to[4]

$$\tan \theta = \frac{h}{G_{200}} \frac{1}{[1 - (h/g_{200})^2]^{1/2}} \tag{32a}$$

$$\text{curvature } C \equiv \frac{K_2}{2ht} = \frac{G_{200}}{2h}\{1 - [1 - (h/g_{200})^2]^{1/2}\} \tag{32b}$$

Two useful expressions for the aspect ratio A_r also arise from the treatment:

$$A_r \equiv \frac{ht + K_3}{G_{200}t} = \frac{h}{G_{200}}\left[1 + \frac{\tan \Lambda}{\tan \theta}\right] \tag{32c}$$

$$A_r = \frac{\tan \theta + \tan \Lambda}{1 + 2C \tan \theta} \tag{32d}$$

To the above may be added the general definition

$$A_r \equiv \frac{G_{110(TIP)}}{G_{200}} = \frac{G_{110}}{G_{200} \cos \Lambda} \tag{32e}$$

The reason for mentioning these alternative forms for A_r will become apparent when we discuss the data of Organ and Keller on polyethylene single crystals. The meaning of the quantities in the above expressions is given in Figure 3.

From eq 32b it is evident that curvature appears only when g_{200} is slightly greater than h. It is for this reason that we earlier sought expressions based on nucleation theory for a substrate completion rate that was comparable in magnitude to the growth rate of a normal facet (in this case G_{110}). It is only when $\sigma_s > 0$ is invoked in this system for the 200-type face that this occurs. In the normal strain-free case, $g_{200} \gg h$, which gives no curvature. The curved edge actually possesses numerous nucleation and growth sites, but nucleation and substrate completion are slow because of the factor $\exp[-4(2^{1/2})b_0\sigma_s\sigma_e/(\Delta G_s)kT]$ in both i and g. On a macroscopic scale, the curved edge is predicted to be the section of an ellipse.[4]

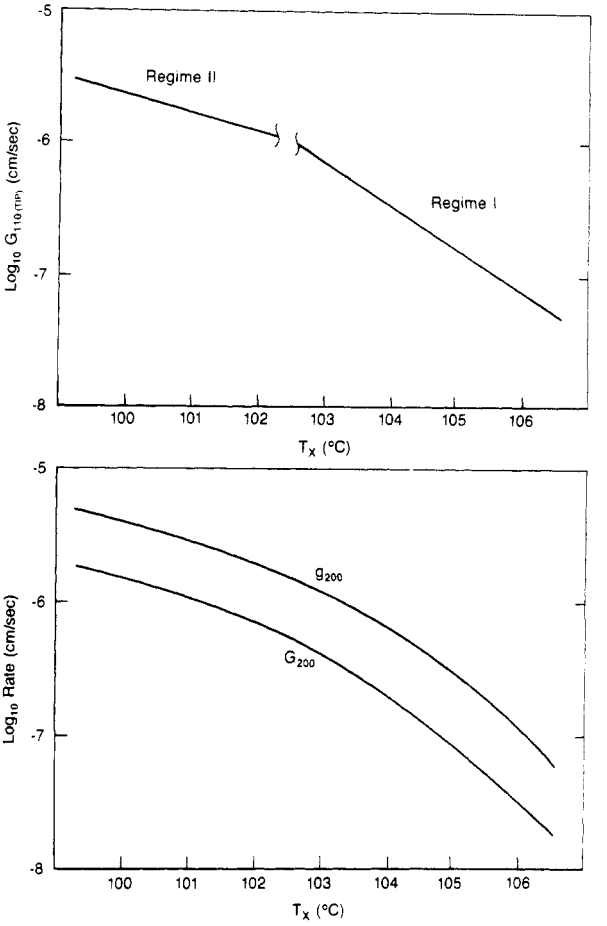

Figure 4. Top: plot of $\log_{10} G_{110(TIP)}$ vs isothermal crystallization temperature T_x for polyethylene single crystals of type shown in Figure 3 formed from 0.05% solution of n-hexadecane (after Organ and Keller[5]). The aspect ratio and the angle θ increase with increasing T_x. Note regime I → II transition associated with 110 facet. Bottom: plot of G_{200} and g_{200} as a function of T_x for same crystals derived from curvature and aspect ratio data of Organ and Keller by using Mansfield's phenomenological equations for g_{200} (see text). Note absence of regime transition in G_{200}. The parallel behavior of G_{200} and g_{200} points directly to the validity of the nonideal serrated surface model. The G_{200} and g_{200} curves depicted are accurately reproduced with $Q_D^* = 2000$ cal mol^{-1}, $\sigma_s = 1.82$ erg cm^{-2}, and $\sigma_{e(200)} \cong 52.5$ erg cm^{-2} ($K_s = 0.174 \times 10^5$ deg^2) in eq 30b and 30d.

In a recent paper, Organ and Keller[5] presented aspect ratio A_r and curvature C data for polyethylene single crystals formed in dilute solution at various isothermal crystallization temperatures T_x. They also gave plots of $\log_{10} G_{110(TIP)}$ vs $1/T(\Delta T)$, which permits the variation of G_{110} with T_x to be established (Figure 4, top) and which allows $K_{g(110)}$ to be found for both regimes I and II. From eq 32e, G_{200} can be obtained directly as a function of T_x. To obtain g_{200}, one first calculates $\tan \theta$ as a function of T_x using the A_r and C data in eq 32d. Then, knowing Λ, $\tan \theta$, A_r, and G_{200}, one calculates h as a function of T_x from eq 32c. Finally, one can obtain g_{200} as a function of T_x with either eq 32a or 32b.

Referring to the data of Organ and Keller on polyethylene crystallized from n-hexadecane (0.05%) for which $T_d = 124.5$ °C, the nature of the overall results can be readily summarized.[6] It was found that G_{200} and g_{200} were smooth functions that descended rapidly with increasing T_x and that almost exactly paralleled one another—g_{200} was everywhere close to 3.0 times faster than G_{200} (Figure

4, bottom). These relatively smooth changes occurred despite the fact that the 110 face exhibited a regime I → II transition. The behavior of G_{200} corresponded to regime II at all T_x. (The 110 face behaved as expected according to the customary flat surface model, with $K_{g(I)} \cong 2K_{g(II)} = 1.129 \times 10^5$ deg^2 giving $\sigma\sigma_{e(110)}$ of ~661 erg^2 cm^{-4}, which is close to the value quoted by Organ and Keller. We used $Q_D^* = 2000$ cal mol^{-1} in our analysis. There is no evidence of a σ_s effect on the 110 face.)

Having found by analysis of data the actual behavior of g_{200} and G_{200} to be as depicted in Figure 4, the problem became that of finding if a nucleation-based model could describe this behavior. Should this be accomplished, one would be assured that the curvature, axial ratio, and tan θ would be predicted as a function of crystallization temperature for the crystals with eq 32. Toward this end, the parallel character of g_{200} and G_{200} over a range of temperature (Figure 4) points directly to the serrated surface model with lattice strain according to eq 30b and 30d.

By a fit of the G_{200} and g_{200} data with eq 30b and 30d, with the help of eq 21c for ΔT_s, it was found for the "square" version of the serrated model that the G_{200} and g_{200} data could be accurately reproduced with $\sigma_{e(200)} \cong 52.5$ erg cm^{-2} and a σ_s of 1.82 ± 0.01 erg cm^{-2}. The value of K_s is (1.74 ± 0.004) × 10^4 deg^2. We found Z_{II}/n in eq 30b to be 4.93×10^{-4} cm s^{-1} deg^{-1} and g_0/nT_m in eq 30d to be 7.87×10^{-3} cm s^{-1} deg^{-1}; T_s is 11.88 °C below T_d. The spacing b_0 for the square version of the model is $(18.9/2)^{1/2}$ or 3.072 Å. No decrease of σ_s with increasing l_g^* could be detected with certainty.

The $\sigma_{e(200)}$ of 52.5 erg cm^{-2} is to be interpreted as a mean fold surface free energy $\bar{\sigma}_{e(200)}$ and corresponds to $\bar{q}_{200} \cong 2.8$ kcal mol^{-1}. The mean *total* work associated with adding a stem onto the substrate of the 200-type edge is $\bar{q}_{200} + 2(2^{1/2})b_0\sigma_s\bar{l}_g$, which has an average value of ~9.0 kcal mol^{-1}. This latter figure may be regarded as the true effective work of chain folding, since both terms are ultimately traceable to the presence of the folds. (Calculations based on the exact values of a_0 and b_0 relevant to the 200 growth front cause σ_s to change slightly, but the energetic quantities quoted above for 200 and such properties as T_s and the calculated $l_{g(200)}^*$ values remain unchanged.) The low $\bar{q}_{200}$ quoted above implies that the "200" fold surface is rather imperfect. Recall that a somewhat reduced degree of "tight" folding may obtain for a serrated surface, which would lower $\sigma_{e(200)}$ and hence $\bar{q}_{(200)}$.

In brief, at the expense of a single additional parameter σ_s in the nucleation-based expressions for G_{200} and g_{200} for the 200-type face as given by eq 30b and 30d, the changes in shape, including the aspect ratio and curvature, were reproduced over the entire range of temperature when these expressions were introduced into the phenomenological formulas given as eq 32. The aspect ratio ranged from ~1.4 at low T_x to ~2.6 at high T_x. In addition, an estimate of the total work of chain folding associated with the folds on the 200-type surface was obtained. Basically similar results were found by using the data of Organ and Keller for polyethylene crystals formed in *n*-tetradecanol, though the different solvent and range of undercooling led to some differences in $\sigma\sigma_{e(110)}$, $\sigma_s\sigma_{e(200)}$, and $\bar{q}_{200}$. For crystals formed in *n*-tetradecanol, where the temperature range studied was larger than for *n*-hexadecane, the anticipated small decrease of σ_s with increasing $l_{g(200)}^*$ was detected.[6]

There are a number of additional points to mention in connection with the treatment of polyethylene single crystals with two types of sectors given above. The first is that the l_g^* values calculated for the two types of sector match very closely over only about the lower half of the range of crystallization temperature. The results imply that the mean angle of tilt in the body of the 200-type sector increases with increasing crystallization temperature. Angles of tilt as high as 34° are known in crystals of this type.[38] Next, the theory predicts that because of the presence of lattice strain in the 200-type sector, it will melt before the 110-type sector on warming even though the two sectors have about the same l_g^* values. The relevant formula derived from eq 2a and 21b is

$$T_{m(100)}' - T_{m(200)}' = (2T_m/\Delta h_f)[(\sigma_{e(200)} - \sigma_{e(110)})/l + 2^{1/2}\sigma_s/2b_0] \quad (33)$$

where $l = l^*_{g(110,200)}$. The calculated difference in melting points is typically 3–5 °C; this prediction assumes that the warming rate is such as to discourage a significant degree of thickening and recrystallization. The main source of the difference is the term involving σ_s. Evidence suggesting that the 200-type sector melts at a significantly lower temperature than the 110 was presented many years ago by Bassett, Frank, and Keller.[39] More recent work by Harrison[40] has fully confirmed this finding. This supports our treatment of the origin of curved edges, since it directly implies the presence of lattice strain in the 200-type sector. The prediction of such "double" melting points is an inherent property of the model. We mention further that, as predicted, the shape of the curved edges seen in polyethylene single crystals appears to be closely approximated by a section of an ellipse as seen where appropriate micrographs are available. The model also explains the fact that the crystals maintain the same shape as they grow. Another observation is that the analysis outlined above shows that different regimes can be active for different sectors of a crystal at the same temperature.

V. Discussion and Conclusions

As treated with the flux equation approach typified by the calculations given in section II with $\sigma_s \to 0$, the flat surface model with lattice strain omitted has played a major role in explaining the origin of chain folding. This approach shows that the initial lamellar thickness l_g^* for this model is determined by the mean rate of passage over the nucleation barrier. The same flux controls the growth kinetics. Together with the "gambler's ruin" calculation, which on topological grounds requires a considerable degree of "tight" folding,[17] one has a basic rationale for why chain folding occurs. Meanwhile, the model leads to detailed expressions that have been widely and successfully used in analysing data. Examples of successful application of the strain-free flat surface model to various types of phenomena associated with chain folding are to be found in ref 1, 2, 9, 14, 20, 21, 23, 30–33, 35, and 41. While this list is far from exhaustive, it is sufficient to raise the question of why this model has such broad applicability.

In light of the present work, the answer to the question posed above must be as follows: (1) the flat surface model is a sufficiently realistic representation of the dominant growth front in many situations, and (2) the fold array associated with the dominant growth front in the type of crystals studied did not involve a serious degree of repulsion such that a large general lattice expansion took place, thus incurring significant lattice strain. Indeed, in the case of polyethylene, the flat surface model with $\sigma_s \to 0$ is adequate to deal with the initial lamellar thickness, growth kinetics, and melting behavior associated with the 110 sector.[1,9,23] However, in the case of the 200 sector in the same crystal, it is clearly evident from the present work that a definite degree of repulsion leading to lattice strain is present. Thus, the degree to which σ_s is present in a given type of sector is dependent on the fold structure

peculiar to that sector. This implies of course that different lattice planes are involved in the two types of sectors. It is clear in the case of polyethylene that this is true. Because we found from an analysis of data using the phenomenological expressions of Mansfield that g_{200} and G_{200} exhibited parallel behaviors over a considerable range of isothermal crystallization temperatures (Figure 4, bottom), it was required that a serrated surface model with a definite σ_s be invoked for the 200-type edge (eq 30b and 30c). The flat surface model cannot give g_{200} and G_{200} with such parallel behavior.

It is worthwhile to look more closely at why a "200"-type sector appeared at all in polyethylene. A serrated surface with no strain has a nil nucleation barrier. In the absence of strain effects, such an edge would fill out very rapidly. However, because of the special nature of the fold array of the 200 sector in the crystal, lattice strain energy was generated that caused the growth rate to become somewhat less than that of the 110 edge. Given the evidence presented here for the presence and magnitude of σ_s in the 200 sector and recalling the behavior of g_{200} when σ_s is large, the curved edge is seen to have a natural origin. One must appreciate, however, that the requirements for the appearance of marked curvature are quite stringent as eq 32b shows—the quantity g_{200} must be just slightly larger than h.

While it has been possible to estimate the absolute value of σ_s from both kinetics and from molecular energy calculations,[13] details of the repulsion effects on the 200 fold surface that lead ultimately to the large σ_s value are not known. It is known from the work of Davé and Farmer[42] that at least one of the more obvious 200 fold configurations, which in isolated form has a normal work of chain folding, develops very strong repulsions with nearby folds when these neighbors are considered. Some such folds may well be involved in generating the expansion of the lattice that leads to the presence of the interfacial surface free energy σ_s. The fact that folds can in special cases lead to interior lattice expansion effects, in addition to the fold energy q characteristic of the surface only, is a topic worthy of detailed investigation from the standpoint of molecular energy calculations.

There was no indication of a δ catastrophe effect or even a premonitory hint thereof in the analysis of the kinetic data for either the 110 or the 200 sectors of the polyethylene single crystals discussed in section IV. Thus the arguments given for low-Ψ and the "partial stem" character of the nucleation process are clearly valid for both types of sector.

The results for both models considered are relatively insensitive to whether the backward reaction (stem removal) is included or not. (The largest quantitative difference occurs in δ for the serrated model ($kT/2(2^{1/2})\sigma_s b_0$ for $\epsilon = 0$, $kT/(2^{1/2})\sigma_s b_0$ for $\epsilon = 1$).) The forward reactions virtually completely dominate the flux and thence all the rate-dependent properties. Because the expressions based on $\epsilon = 1$ and $\epsilon = 0$ are so similar, it will doubtless be difficult to determine on experimental grounds whether the nucleation process involved in chain folding is steady-state or non-steady-state in character. The possibility that crystallization with chain folding may take place under non-steady-state conditions at high undercoolings deserves consideration.

It is interesting that the surface models found useful in analyzing data up to the present represent extremes or only modest departures from these extremes. We have already noted the success of the flat surface model (without large strain effects) in treating situations relating to a dominant growth front. Similarly, the quite different serrated surface model with marked strain effects but with little or no flat surface character appears to explain the unusual "curved edge" behavior of an auxiliary growth front. Intermediate surface types are conceivable and may be required in the future. The properties associated with them can readily be calculated by using the methods described here.

Overall Summary. The present work removes the concern that nucleation theory could not deal with the problem of curved edges, at least with regard to those seen in polyethylene single crystals formed in dilute solution. The methods used were well within the spirit of nucleation theory. Basically what was added was the effect of lattice strain and calculations for a growth front with a different molecular geometry than had been employed heretofore. The curved edge of the 200 sector in polyethylene single crystals, which is of the serrated surface type, originates from chain fold repulsions that lead to lattice strain effects characterized by an interfacial surface free energy σ_s; these effects in turn depress the melting point and slow down the substrate completion rate for that sector to the point that the latter is only slightly greater than the rate of advance of the adjoining 110 sector. Besides predicting the curvature of the 200 edge and the axial ratio of the crystals as a function of crystallization temperature, the theory with σ_s also offers an explanation of the "double" melting points exhibited by crystals with both 110 and 200 sectors. For all the models treated (flat and serrated), the initial lamellar thickness and the nucleation rate were controlled by the net flux across the nucleation barrier. The primacy of the forward reactions in determining flux-based properties is shown. A more detailed picture of the apportionment factor Ψ is provided, showing that only part of a stem is crystallographically attached at the point in time that the activated state for the forward reaction is attained (partial stem character of activated state). The basic cause of chain folding is the same for the serrated surface model and the flat surface model. Except for special situations of the type represented by the curved 200 edge in polyethylene where the serrated surface model with lattice strain must be invoked, the flat surface model and the expressions relating thereto retain their broad utility.

Acknowledgment. We are indebted to Dr. Marc L. Mansfield of Michigan Molecular Institute for helpful suggestions and for communicating his work on curved edges to us prior to publication. We are also indebted to Dr. Freddy Khoury of the National Bureau of Standards for much helpful comment and advise. This work was partially supported (J.D.H.) by Grant DMR 86-07707 of the Division of Materials Research, Polymer Program, of the National Science Foundation.

Appendix A. Flat Surface Model with Lattice Strain: General Case for a Fully Active Backward Reaction ($\epsilon = 1$) and a Truncated Backward Reaction ($\epsilon = 0$)

Here we outline the calculation of i, g, and l_g^* for the flat surface model for the situation where the backward reaction has a range of activity ($0 \leq \epsilon \leq 1$). Although the emphasis will be on the $\epsilon = 1$ case, corresponding to a fully active backward reaction with detailed balance, it is considered instructive to carry out the calculations in a more general framework that also encompasses the case $\epsilon = 0$ as well as intermediate ones. The expressions for i, g, and l_g^* obtained below for the $\epsilon = 1$ case are those employed with eq 17–19 to express G_I, G_{II}, and G_{III} as given in Table I. We employ starting formulas based on the approxi-

mation $\Psi = 0$, which gives results that are applicable at all but very large undercoolings (cf. eq 5).

We begin with the practical rate expressions, eq 6. With these expressions the flux (eq 8a) is found to be

$$S(l) \equiv \frac{N_0 A_0 (A - B)}{A - B + B_1} = N_0 \beta e^{-[2b_0\sigma + a_0\sigma_s]l/kT}[1 - \epsilon e^{q/kT} e^{-a_0 b_0 l(\Delta G_s)/kT}] \quad \text{(A1)}$$

The total flux S_T is

$$S_T \equiv \frac{1}{l_u}\int_{2\sigma_e/\Delta G_s}^{\infty} S(l)\, dl = \frac{N_0\beta}{l_u}(M - \epsilon N) e^{[-[2b_0\sigma + a_0\sigma_s]/kT](2\sigma_e/\Delta G_s)} \quad \text{(A2)}$$

where

$$M = \frac{kT}{2b_0\sigma + a_0\sigma_s} \quad \text{(A3)}$$

$$N = \frac{kT}{2b_0\sigma + a_0\sigma_s + a_0 b_0 (\Delta G_s)} \quad \text{(A4)}$$

Both M and N are in units of length. With $i \equiv S_T/n_L a_0$ and $N_0 = C_0 n_L$ as before

$$i = \left(\frac{C_0}{a_0}\right)\beta\left(\frac{M - \epsilon N}{l_u}\right) e^{[-[2b_0\sigma + a_0\sigma_s]/kT](2\sigma_e/\Delta G_s)} \quad \text{(A5)}$$

For the case $\epsilon = 1$ there is obtained

$$i = \frac{C_0}{a_0}{}^1\beta\left[\frac{kT a_0 b_0 (\Delta h_f)}{(2b_0\sigma + a_0\sigma_s)^2 l_u}\right]\left(\frac{\Delta T_s}{T_m}\right) e^{[-[2b_0\sigma + a_0\sigma_s]/kT](2\sigma_e/\Delta G_s)} \quad \text{(A6)}$$

In the exponent we let $(a_0/2b_0)\sigma_s \rightarrow \sigma_s/2$, and in the preexponential we let $\sigma \gg \sigma_s$ as before. Then the practical nucleation rate for $\epsilon = 1$ becomes

$$i \cong \frac{C_0}{a_0}{}^1\beta\left(\frac{kT}{2b_0\sigma l_u}\right)\left(\frac{a_0(\Delta h_f)}{2\sigma}\right)\left(\frac{\Delta T_s}{T_m}\right) e^{-4b_0[\sigma + \sigma_s/2]\sigma_e/(\Delta G_s)kT} \quad \text{(A7)}$$

The results in Table I for $\epsilon = 1$ are based on this expression. The value of ${}^1\beta$ required in these calculations is[9]

$${}^1\beta = \left(\frac{{}^1\kappa}{n}\right)\left(\frac{kT}{h}\right) e^{-Q_D^*/RT} \quad \text{(A8)}$$

where

$${}^1\kappa = \left(\frac{h}{kT}\right)\frac{b_0\sigma \exp(Q_D^*/RT_0)}{\zeta_0 l_f} \quad \text{(A9)}$$

Note that if ϵ is taken as zero in the general expression A5, eq 12 of the main text is found. With the rate-averaging law for l_g^* expressed in eq 14 together with eq A1, A3, and A4, one finds for the case of general ϵ

$$l_g^* = \frac{2\sigma_e}{\Delta G_s} + \frac{M^2 - \epsilon N^2}{M - \epsilon N} = \frac{2\sigma_e}{\Delta G_s} + \delta \quad \text{(A10)}$$

For the case $\epsilon = 1$, the expression for δ is exactly

$$\delta = M + N = \frac{kT}{2b_0\sigma + a_0\sigma_s}\left\{\frac{\frac{2[2b_0\sigma + a_0\sigma_s]}{a_0 b_0} + (\Delta G_s)}{\frac{[2b_0\sigma + a_0\sigma_s]}{a_0 b_0} + (\Delta G_s)}\right\} \quad \text{(A11)}$$

Since at normal undercoolings ΔG_s is considerably smaller than $2[2b_0\sigma + a_0\sigma_s]/a_0 b_0 \cong 4\sigma/a_0$, one has to an excellent approximation with $(a_0/2b_0)\sigma_s \rightarrow \sigma_s/2$ in the leading term

$$l_g^* \cong \frac{2\sigma_e}{\Delta G_s} + \frac{kT}{b_0(\sigma + \sigma_s/2)} \quad \text{(A12)}$$

for the $\epsilon = 1$ calculation where the backward reaction is fully active. For many applications, the approximation $\delta = kT/b_0\sigma$ is entirely satisfactory. Observe that eq A10 with $\epsilon = 0$ yields the result for l_g^* quoted as eq 15b of the text.

The substrate completion rate is given in general by

$$g \equiv a_0(A - B) = a_0\beta e^{-q/kT} e^{-(a_0 + b_0)\sigma_s l/kT}[1 - \epsilon e^{q/kT} e^{-a_0 b_0 l(\Delta G_s)/kT}] \quad \text{(A13)}$$

For the case $\epsilon = 1$, we let $l = 2\sigma_e/(\Delta G_s) + \delta$ and expand the exponential involving δ to obtain

$$g = a_0{}^1\beta\left[\frac{a_0 b_0 \delta(\Delta G_s)}{kT}\right] e^{-q/kT} e^{-2(a_0 + b_0)\sigma_s\sigma_e/(\Delta G_s)kT} e^{-(a_0 + b_0)\sigma_s\delta/kT} \quad \text{(A14)}$$

Setting $\exp[-(a_0 + b_0)\sigma_s\delta]/kT$ equal to unity and inserting $\delta = kT/b_0\sigma$, one has

$$g = a_0{}^1\beta\left[\frac{a_0(\Delta h_f)}{\sigma}\right]\left[\frac{\Delta T_s}{T_m}\right] e^{-q/kT} e^{-2(a_0 + b_0)\sigma_s\sigma_e/(\Delta G_s)kT} \quad \text{(A15)}$$

This may be written with (A8) as

$$g = a_0\left(\frac{{}^1\kappa}{n}\right)\left(\frac{kT}{h}\right)\left(\frac{a_0(\Delta h_f)}{\sigma}\right) \times \left(\frac{\Delta T_s}{T_m}\right) e^{-Q_D^*/RT} e^{-q/kT} e^{-2(a_0 + b_0)\sigma_s\sigma_e/(\Delta G_s)kT} \quad \text{(A16)}$$

When combined with ${}^1\beta$ as given in eq A8 and A9, which calibrates the substrate completion rate in accord with reptation theory,[9] one finds the alternative form for the $\epsilon = 1$ case

$$g = (g_0/n)(\Delta T_s) e^{-Q_D^*/RT} e^{-q/kT} e^{-2(a_0 + b_0)\sigma_s\sigma_e/(\Delta G_s)kT} \quad \text{(A17)}$$

where $g_0 = [a_0{}^2 b_0(\Delta h_f)/\zeta_0 l_f](1/T_m)\exp(Q_b^*/RT_0)$. (A16) and (A17) are given in Table I as g for the $\epsilon = 1$ case. The expressions for g for the case $\epsilon = 0$ given in the main text are readily found beginning with eq A13.

Appendix B. Semiempirical Treatment of Behavior of ϵ with Undercooling

Let

$$\epsilon = 1 - e^{-t/\tau} \quad \text{(B1)}$$

where t = lifetime of a stem in a niche, and τ = mean time required for a stem at a niche to be detached. Further, let the lifetime t be of the form

$$t = a_0/g \cong a_0/\Gamma(\Delta T) \quad \text{(B2)}$$

where a_0 is the width of a stem in centimeters and g is the substrate completion rate in cm s^{-1}. The second equality in eq B2 recognizes the fact that the substrate completion rate for a considerable temperature range near the melting point varies approximately as ΔT for the case $\sigma_s \rightarrow 0$.

Then

$$\epsilon = 1 - e^{-a_0/\Gamma\tau(\Delta T)} \quad \text{(B3)}$$

This expression gives $\epsilon \rightarrow 1$, i.e., detailed balance as $\Delta T \rightarrow 0$ as required. However it leads to very small ϵ values at large ΔT if $\tau > t$. For the example of melt-crystallized polyethylene in the text where g_{110} is given in eq 7, it is readily found that Γ is $5.32 \times 10^{-3}/n$ cm s^{-1} deg^{-1}, or 1.77

$\times 10^{-6}$ cm s^{-1} deg^{-1} for $n = 3000$. With $a_0 = 4.55 \times 10^{-8}$ cm this yields

$$\epsilon = 1 - e^{-0.0257/\tau(\Delta T)} \quad \text{(B4)}$$

The assumption $\sigma_s \cong 0$ is clearly valid for the 110 face. With τ set at 0.1 s, this gives $\epsilon = 1$ at $\Delta T = 0$, $\epsilon = 0.015$ at $\Delta T = 16.5$ °C, and $\epsilon = 0.009$ at $\Delta T = 30$ °C. The value of τ employed in this example is arbitrary. The value employed is simply meant to reflect the idea that, by analogy with the known slow desorption rates of chains from surfaces, the detachment time may be quite long compared to t. This illustrative example serves to show that if the stem detachment time τ is increased by statistical events of the type possible in chain systems, large departures from detailed balance leading to non-steady-state nucleation with $\epsilon \rightarrow 0$ can result at sufficiently large ΔT. For the flat surface model one can adjust τ such that $\delta \sim kT/b_0\sigma$ at high T_x in regime I and $\delta \sim kT/2b_0\sigma$ at low T_x in regime III (see eq A10).

Registry No. Polyethylene, 9002-88-4.

References and Notes

(1) Hoffman, J. D.; Davis, G. T.; Lauritzen, J. I., Jr. In *Treatise on Solid State Chemistry*; Hannay, N. B., Ed.; Plenum Press: New York, 1976; Vol. 3, Chapter 7.
(2) Passaglia, E.; Khoury, F. *Polymer* **1984**, *25*, 631.
(3) Sadler, D. M. *Polymer* **1987**, *28*, 1440.
(4) Mansfield, M. L. *Polymer* **1988**, *29*, 1755.
(5) Organ, S. J.; Keller, A. *J. Polym. Sci., Part B: Polym. Phys.* **1986**, *24*, 2319.
(6) Miller, R. L.; Hoffman, J. D., to be submitted for publication in *Polymer*.
(7) Lauritzen, J. I., Jr.; Hoffman, J. D. *J. Res. Natl. Bur. Stand., Sect. A* **1960**, *64*, 73.
(8) Frank, F. C.; Tosi, M. *Proc. R. Soc. London, Ser. A* **1961**, *263*, 323.
(9) Hoffman, J. D.; Miller, R. L. *Macromolecules* **1988**, *21*, 3038.
(10) Guttman, C. M.; DiMarzio, E. A. *J. Appl. Phys.* **1983**, *54*, 5541.
(11) Bassett, D. C.; Olley, R. H.; Al Raheil, I. A. M. *Polymer* **1988**, *29*, 1539.
(12) Davis, G. T.; Weeks, J. J.; Martin, G. M.; Eby, R. K. *J. Appl. Phys.* **1974**, *45*, 4175.
(13) Marand, H. *Macromolecules*, in press.
(14) Hoffman, J. D. *Macromolecules* **1986**, *19*, 1124.
(15) Guttman, C. M.; DiMarzio, E. A.; Hoffman, J. D. *Polymer* **1981**, *22*, 1466.
(16) Guttman, C. M.; DiMarzio, E. A. *Macromolecules* **1982**, *15*, 525.
(17) In ref 15 and 16 it is shown by the "gambler's ruin" method that the probability of "tight" folding on a lamellar surface p_{tf} is bounded by $p_{tf} \geq 1 - (\rho_a/\rho_c)(l_b/l_u)[1/(3 \cos \phi)]$. Here ρ_a = density of liquid, ρ_c = density of crystal, l_b = bond length, l_u = length of monomer unit, and ϕ = angle of tilt as measured from the vertical. Violation of this expression leads to a density paradox at the lamellar surface. (The criterion for a "tight" fold is that the reentry be closer than $C_\infty l_b$, where C_∞ = characteristic ratio; this defines "very near adjacent" as a reentry within ca. 10 Å in polyethylene.) For polyethylene $(\rho_a/\rho_c)(l_b/l_u)$ is 0.85 (1.54 Å/1.27 Å) = 1.03. For $\phi = 0$ (vertical stems) $p_{tf} = 0.657$, and for $\phi = 34°$ $p_{tf} \geq 0.586$. Similar though less quantitative conclusions were reached earlier by a different method: Frank, F. C. *Faraday Discuss. Chem. Soc.* **1979**, *No. 68*, 7.
(18) Mansfield, M. L. *Macromolecules* **1983**, *16*, 914.
(19) Guttman, C. M.; DiMarzio, E. A.; Hoffman, J. D. *Polymer* **1981**, *22*, 597. Sadler, D. M. In *Static and Dynamic Properties of the Polymeric Solid State*; Pethrick, R. A., Richards, R. W., Eds.; Reidl: London, 1982; p 81.
(20) Lauritzen, J. I., Jr.; Hoffman, J. D. *J. Appl. Phys.* **1973**, *44*, 4340.
(21) Hoffman, J. D. *Polymer* **1982**, *23*, 656.
(22) Jones, D. H.; Latham, A. J.; Keller, A.; Giralomo, M. J. *J. Polym. Sci., Polym. Phys. Ed.* **1973**, *11*, 1759.
(23) Miller, R. L. *Kolloid Z. Z. Polym.* **1968**, *225*, 62.
(24) Stromberg, R. R.; Grant, W. H.; Passaglia, E. *J. Res. Natl. Bur. Stand., Sect. A* **1964**, *68*, 391.
(25) This explanation for the sluggish rate of polymer desorption was pointed out to J.D.H. many years ago by Prof. E. Passaglia, Johns Hopkins University.
(26) Hoffman, J. D. *Polymer* **1985**, *26*, 803.
(27) Organ, S. J.; Keller, A. *J. Polym. Sci., Part C: Polym. Lett.* **1987**, *25*, 67.
(28) Leung, W. M.; Manley, R. St. J.; Panaras, A. R. *Macromolecules* **1985**, *18*, 760.
(29) DiMarzio, E. A.; Guttman, C. M.; Hoffman, J. D. *Faraday Discuss. Chem. Soc.* **1979**, *No. 68*, 210.
(30) Hoffman, J. D. *SPE Trans.* **1964**, *4*, 315.
(31) Suzuki, T.; Kovacs, A. J. *Polym. J. (Tokyo)* **1970**, *1*, 82.
(32) Hoffman, J. D.; Weeks, J. J. *J. Chem. Phys.* **1962**, *37*, 1723.
(33) Frank, F. C. *J. Cryst. Growth* **1974**, *22*, 233.
(34) Lauritzen, J. I., Jr. *J. Appl. Phys.* **1973**, *44*, 4353.
(35) Hoffman, J. D. *Polymer* **1983**, *24*, 3. For an earlier discussion of regime III, see: Hoffman, J. D.; Guttman, C. M.; DiMarzio, E. A. *Faraday Discuss. Chem. Soc.* **1979**, *No. 68*, p 177. Hoffman, J. D. *Ibid* 378 ff.
(36) Klein, J.; Ball, R. *Faraday Discuss. Chem. Soc.* **1979**, *No. 68*, 198.
(37) Wittmann, J. C.; Lotz, B. *J. Polym. Sci., Polym. Phys. Ed.* **1985**, *23*, 205.
(38) Khoury, F.; Bolz, L. H. *Proc.—Annu. Meet., Electron Microsc. Soc. Am.* **1980**, *38*, 242. See also: Khoury, F. *Faraday Discuss. Chem. Soc.* **1979**, *No. 68*, 404.
(39) Bassett, D. C.; Frank, F. C.; Keller, A. (a) *Nature* **1959**, *184*, 810; (b) *Proc. Eur. Reg. Conf. Electron Microsc., 2nd* **1960**, *1*, 244.
(40) Harrison, I. R. (a) *J. Polym. Sci., Polym. Phys. Ed.* **1973**, *11*, 991; (b) *J. Macromol. Sci., Chem.* **1974**, *A8*, 43.
(41) Clark, E. J.; Hoffman, J. D. *Macromolecules* **1984**, *17*, 878.
(42) Davé, R. S.; Farmer, B. L. *Polymer* **1988**, *29*, 1544.